Galactic Winds

Sylvain Veilleux
Department of Astronomy, University of Maryland, College Park, MD 20742; E-mail: veilleux@astro.umd.edu

Gerald Cecil
Department of Physics and Astronomy, University of North Carolina, Chapel Hill, NC 27599-3255; E-mail: cecil@physics.unc.edu

Joss Bland-Hawthorn
Anglo-Australian Observatory, Epping, NSW, Australia; E-mail: jbh@aaoepp.aao.gov.au

Key Words galaxies: evolution — galaxies: halos — galaxies: intergalactic medium — galaxies: kinematics and dynamics — galaxies: nuclei

Abstract Galactic winds are the primary mechanism by which energy and metals are recycled in galaxies and are deposited into the intergalactic medium. New observations are revealing the ubiquity of this process, particularly at high redshift. We describe the physics behind these winds, discuss the observational evidence for them in nearby star-forming and active galaxies and in the high-redshift universe, and consider the implications of energetic winds for the formation and evolution of galaxies and the intergalactic medium. To inspire future research, we conclude with a set of observational and theoretical challenges.

CONTENTS

INTRODUCTION 2
Fundamental role 2
Early History 3
Review structure 4

BASIC PHYSICS 4
Sources of Energy 4
Wind-blown bubbles 7
Galactic winds 9
Hydrodynamical Simulations 10

MAJOR WINDBLOWN EVENTS IN THE LMC & GALAXY 11
Large Magellanic Cloud 11
Nuclear Wind in the Galaxy 12

LOCAL CENSUS OF GALACTIC WINDS IN STAR-FORMING GALAXIES . . 13
Search Techniques & Observational Limitations 13
Detection Rate 14
Morphology 15
Kinematics 18
Mass Outflow Rates & Energetics 19
Escape Fraction 21
Energy Injection Zone 22
Excitation Properties & Evolution 23
Wind Fluid 23
Dust 24

LOCAL CENSUS OF LARGE-SCALE OUTFLOWS IN ACTIVE GALAXIES . . 25
Detection Rate 26
Morphology 27
Kinematics 28
Mass Outflow Rates & Energetics 30
Energy Injection Zone 31
Source of Ionization 32
Dust 32

WINDS IN THE DISTANT UNIVERSE 32
High-Redshift Galaxies 32
QSO Absorption-Line Systems 34

THE SIGNIFICANCE OF GALACTIC WINDS 35
Influence of Winds on Galactic Scales 35
Influence of Winds on Intergalactic Scales 38

FUTURE DIRECTIONS 39
Observational Challenges 39
Theoretical Challenges 42

1 INTRODUCTION

1.1 Fundamental role

On the largest physical scales, the Universe is shaped by gravity and the dark energy. On galactic scales, gravity is responsible for only part of what we see through telescopes. This has become clear from the most comprehensive numerical simulations involving up to 10^{10} particles, which purport to track the evolution of individual galaxies to the present day. Although Cold Dark Matter (CDM) simulations account well for the observed large-scale structure, problems emerge in regions of high-density and high density contrast. Even the most detailed simulations do not explain adequately what we know of galaxies.

Contemporary astrophysics is entering a new era where a proper understanding of galaxy formation and evolution forces us to confront details of physical processes involved in feedback, including star formation and evolution, energetic and chemical recycling in the interstellar and intergalactic media (ISM, IGM), gas dynamics, and ultimately plasma magnetohydrodynamics. Progress is complicated by: (i) the need for comprehensive data over the full electromagnetic spectrum at comparable sensitivity and spatial resolution; and (ii) a lack of detailed theoretical

and numerical models that can accommodate the multi-wavelength observations.

In this review, we confront arguably the dominant feedback in galaxy formation and evolution — galactic winds (GWs). Also important is radiative feedback. But even here, outflows likely play a key role in clearing a path for the escaping radiation (e.g., Dove, Shull, & Ferrara 2000).

1.2 Early History

More than forty years ago, Lynds & Sandage (1963) announced 'evidence for an explosion in the center of the galaxy M82.' In the following year, Burbidge, Burbidge, & Rubin (1964) remarked that 'the activity in M82 is yet another manifestation of the generation of vast fluxes of energy by processes which are not yet properly understood.' This comment echoed the discovery of the first quasar in 1962, and the slow realization that many extragalactic radio sources must be enormously energetic, powered by processes that could only be guessed at (Hoyle & Fowler 1963). However, these seminal papers note important similarities between M82 and the Crab nebula when comparing their optical and radio properties, and they imply a possible role for nuclear star clusters in driving the central explosion. By the end of the decade, black holes (BHs) were identified as the driving mechanism in quasars and powerful radio sources (Lynden-Bell 1969).

Before the discovery of a central explosion in M82, few workers discussed galactic outflows. The observed corona and radio halo in the Galaxy (Spitzer 1956; Baldwin 1955) motivated Burbidge & Hoyle (1963) to consider whether such a halo was in fact bound to the Galaxy. In 1957, van Woerden, Rougoor & Oort provided the first evidence of outflowing gas from the Galactic Center, and identified an 'expanding arm.' Starting with Moore & Spiegel (1968), many authors went on to consider the possibility of a central explosion to power the radial outflow (e.g., van der Kruit 1971; Sanders & Prenderghast 1974; Oort 1977).

In a parallel development, after the detection of broad [O II] λ3727 emission in some elliptical galaxies by Osterbrock (1960), Burke (1968) suggested the presence of a galaxy-scale wind. Interest in GWs continued and models grew in sophistication, motivated largely by the observation that ellipticals have very little ISM and therefore may have been swept clean by galaxy-scale outflows (Johnson & Axford 1971; Mathews & Baker 1971).

Over the past 40 years almost the entire electromagnetic spectrum has become accessible, and we have become aware of the ubiquity of GWs. Their study is now a key area of research, and advances in ground-based and spaceborne instrumentation have produced a flurry of high-precision data on spatially resolved winds in nearby galaxies. At low redshift, winds in gas-rich galaxies are studied because the dense ISM accentuates the outflow. The most recent development is the discovery of powerful winds in high-redshift galaxies. These new observations strongly implicate wind-related feedback processes as key to the chemical and thermal evolution of galaxies and the IGM.

1.3 Review structure

Despite the importance of this topic, there has never been a comprehensive review of GWs published in the *Annual Reviews of Astronomy and Astrophysics*, although articles on closely related topics were written by Tenorio-Tagle & Bodenheimer (1988) on superbubbles and Spitzer (1990) on the hot ISM.

It is only recently that astronomers have been able to compile multiwavelength data on a significant sample of galactic winds. We recognize the need for these observations to be discussed within a universal framework, where hydrodynamical CDM simulations are able to predict the onset of galactic winds and track their evolution in different environments. However, numerical models that give repeatable results at different resolution scales (e.g. mass) have only recently become possible and the published results are limited at the present time (Springel & Hernquist 2003).

The principal goals of our review are to use both observational constraints and theoretical predictions to discuss critically the properties of GWs in the local and distant universe, and to evaluate the importance of these winds for the formation and evolution of galaxies and the IGM. We focus on material published within the past 15 years. Our discussion centers on three fundamental issues:

- *Their Nature.* What are they? Which conditions trigger them? What powers them: star clusters or BHs? Are they nuclear or disk-wide? How energetic are they − are they relatively quiescent or explosive? What mass, momentum, energy, and metals do they transport? How far?
- *Their Frequency of Occurrence.* How common were they in the past and are they now? What is their duty cycle? When did they begin to blow?
- *Their Impact.* How important are they? What impact do they have on the nucleus, bulge, disk, halo, and dark matter of the host galaxy? Are they the dominant source of feedback in galaxy evolution? How do they influence the intergalactic environment? What are their fossil signatures?

Section 2 outlines the basic physics behind the GW phenomenon, and presents several useful formulae and prescriptions to help with data interpretation. Sections 3, 4 and 5 provide an observational summary of wind-blown events in local star-forming and active galaxies. Section 6 summarizes the results from surveys at high redshifts, and §7 discusses the impact of winds on the galactic and intergalactic environments. In the last section (§8), we raise some important, unanswered questions and suggest future directions for research.

2 BASIC PHYSICS

2.1 Sources of Energy

The central question of what powers a GW dates back forty years to the discovery of the wind in M82. For reasons to be discussed in §5.1, remarkably few winds are unambiguously AGN (active galactic nucleus) or starburst driven. Hence, we now summarize the basic physics behind both kinds of energy sources.

2.1.1 STELLAR WINDS & SUPERNOVAE Starburst winds are driven by the mechanical energy and momentum from stellar winds and supernovae (SNe). Models that synthesize the evolution of populations of massive stars have estimated the mass and energy returned from starbursts (e.g., Leitherer, Robert, & Drissen 1992; Leitherer & Heckman 1995; Leitherer et al. 1999, *Starburst99*). This technique combines stellar evolutionary models, atmospheric models, and empirical spectral libraries to determine the observable properties of the starbursting population. A wide parameter space is explored by varying the shape and mass limits of the stellar initial mass function (IMF), the metallicity, and the star formation rate (SFR) history (e.g., instantaneous burst or constant SFR). Stellar evolutionary models have reproduced successfully most properties of Wolf-Rayet (WR) stars, but overpredict WR mass-loss rates. In general, combined empirical results and theoretical predictions are used instead of model-derived mass-loss rates (Leitherer et al. 1992). For an instantaneous starburst, winds from OB stars dominate early on ($\lesssim 3$ Myr); next come WR stars with mass-loss rates ~ 10 times higher (~ 3 – 6 Myr); and finally, core-collapse Type II SNe dominate until ~ 40 Myr when the least massive (~ 8 $M_\odot$) ones explode.

Figures 107, 108, 113, and 114 from Leitherer et al. (1999) show the time evolution of the mass-loss rates and mechanical luminosities calculated using *Starburst99* for two different starburst histories and various metallicities. In the solar-metallicity case where the mass-loss rate and mechanical luminosity are constant beyond ~ 40 Myr and scale with SFR,

$$\dot{M}_* = 0.26\ (SFR/M_\odot\ \mathrm{yr}^{-1})\ \ M_\odot\ \mathrm{yr}^{-1} \tag{1}$$

$$\dot{E}_* = 7.0 \times 10^{41}\ (SFR/M_\odot\ \mathrm{yr}^{-1})\ \ \mathrm{erg\ s}^{-1}. \tag{2}$$

Because $\dot{p}_* = \dot{M}_* V_* = \sqrt{2\dot{M}_* \dot{E}_*}$, the rate of momentum injection from SNe and stellar winds into the environment can be calculated:

$$\dot{p}_* = 5 \times 10^{33}\ (SFR/M_\odot\ \mathrm{yr}^{-1})\ \ \mathrm{dyne}. \tag{3}$$

In these expressions, the supernova rate $\approx\ 0.02\ (SFR/1\ M_\odot\ \mathrm{yr}^{-1})\ \ \mathrm{yr}^{-1}$.

For comparison, the starburst's radiation pressure, $\tau L_{\mathrm{bol}}/c$, is

$$\dot{p}_{\mathrm{rad}} = 1.3 \times 10^{34}\ \tau L_{\mathrm{bol},11}\ \ \mathrm{dyne}, \tag{4}$$

where $L_{\mathrm{bol},11}$ is the bolometric luminosity of the starburst in units of 10^{11} $L_\odot$ and τ is the optical depth to radiation. In luminous IR galaxies where $L_{\mathrm{bol}} \approx L_{\mathrm{IR}}(8 - 1000\mu\mathrm{m}) \geq 10^{11} L_\odot$ and

$$SFR \approx 17\ L_{\mathrm{IR},11}\ \ M_\odot\ \mathrm{yr}^{-1} \tag{5}$$

(Kennicutt 1998), the radiation pressure in the optically thick case ($\tau = 1$) can be comparable to the pressure from the stellar ejecta.

In general, stellar winds are important only in young ($\lesssim 10^7$ yr) starbursts that form many high-mass ($\gtrsim 60$ $M_\odot$) stars in a metal-rich ($Z > Z_\odot$) environment. In any other situation, SN explosions dominate the energetics of the ISM. SN

explosions usually dominate by the time GWs develop, but stellar winds may be important in superbubbles. Because the star formation activity in a starburst is highly correlated spatially, the ejecta from hot stars and SNe in the starburst region quickly interact through shocks, and mix with the surrounding gas to produce a cavity of hot, metal-enriched material. The thermalization efficiency is the percentage of the mechanical energy from the starburst that heats the gas. Unfortunately, as we show in §3 and §4, this quantity is poorly constrained by observations. Hydro simulations (§2.4) often assume it is 100%, *i.e.* none of the energy injected by the starburst is radiated away. In reality, this efficiency is set by the environment, particularly by the gas density, and may be $\lesssim 10\%$ in the dense cores of powerful nuclear starbursts (e.g., Thornton et al. 1998; Silich, Tenorio-Tagle, & Muñoz-Tuñón 2003; Stevens & Hartwell 2003; Melioli & de Gouveia Dal Pino 2004). Conversely, large SN rates may increase the porosity of the ISM, and hence reduce radiative energy losses (e.g., Larson 1974; Cantó, Raga, & Rodriguez 2000; Wada & Norman 2001). Current data favor values $\gtrsim$ 10% for the thermalization efficiency (see §4.5).

2.1.2 AGN The ubiquity of supermassive BHs at the center of galaxies (e.g., Kormendy & Gebhardt 2001) suggests that BH activity may also power some galactic-scale outflows by accretion:

$$\dot{E} \simeq 10^{11}\ (\epsilon/0.01)\ \dot{M}_{\rm acc}\ \ L_\odot, \tag{6}$$

where $\dot{M}_{\rm acc}$ is the mass accretion rate in $M_\odot$ yr^{-1} and ϵ, the energy conversion efficiency in rest mass units. The mass accretion rate ranges from $\lesssim 0.001$ $M_\odot$ yr^{-1} for low-luminosity AGN, ~ 1 $M_\odot$ yr^{-1} for Seyfert galaxies, and ~ 100 $M_\odot$ yr^{-1} for quasars and powerful radio galaxies. The parameter ϵ depends on BH spin and the boundary conditions near the event horizon, and can reach $\epsilon \approx 0.4$ (e.g., Krolik 1999; Agol & Krolik 2000). Much of the energy released during accretion may be tapped to drive a GW; this can occur through several processes.

Radiative processes may be important in luminous AGN such as Seyfert galaxies and quasars. Radiation can push on the surrounding gas via electron scattering, scattering and absorption on dust grains, photoionization, or scattering in atomic resonance lines. The last one is important for O-star winds and is suspected to be responsible for fast ($\sim 0.03\ c$) outflows in broad absorption-line quasars (BAL QSOs) (Crenshaw, Kraemer, & George 2003). In terms of dynamics, the small opacity to electron scattering ($\kappa_{es} = 7 \times 10^{-25} x$ cm^2 per hydrogen atom, with x the ionization fraction) makes this process unimportant relative to radiation pressure acting on dust grains (effective opacity $\kappa_d \sim 10^{-21}$ cm^2 per H atom), unless the material under consideration is within the dust sublimation radius, $r_{\rm subl} \approx 1\ \sqrt{L_{46}}$ pc (L_{46} is the UV/soft X-ray luminosity in units of 10^{46} erg s^{-1}), and the dust temperature exceeds $T_{\rm subl} \approx 1200$ K. Dopita et al. (2002) have shown that dust absorption dominates over photoelectric absorption when $U \gtrsim \alpha_{\rm B}/(c\kappa_d) \sim 0.01$, where $\alpha_{\rm B}$ is the Case B recombination rate to excited states of hydrogen (Osterbrock 1989) and U is the ionization parameter, *i.e.* the ratio of photon to electron number density. Radiation pressure on dust is therefore probably unimportant in low-luminosity AGN and low-ionization nuclear

emission-line regions (LINERs) where $U \lesssim 10^{-4}$ (e.g., Ferland & Netzer 1983; Veilleux & Osterbrock 1987). However, it may dominate the dynamics of narrow emission-line regions (NLRs) in Seyferts and quasars (see §5.3) and may be responsible for the similarity of the ionization parameter in these objects ($U \approx 0.01$; Dopita et al. 2002).

Radiative heating may also be dynamically important in luminous AGN. Krolik, McKee, & Tarter (1981) found that gas at $T \gtrsim 10^{4.5}$ K, when exposed to the hard power-law radiation of the AGN, undergoes runaway heating if $U \gtrsim 10 - 25$. The result is a gas phase at $T \approx 10^6 - 10^7$ K in which Compton cooling balances inverse Compton heating. The sound speed of this gas, $c_s = \sqrt{kT/\mu m_p} \approx 300\ (T/10^7\ K)^{\frac{1}{2}}$ km s^{-1}, exceeds the rotation velocity of typical galaxies. So, gas subject to runaway heating may expel a wind from the host galaxy (Begelman 1985). Given the condition on U, this wind must originate near the nucleus, being fed by gas from the accretion disk itself or nearby (Begelman, McKee, & Shields 1983; Balsara & Krolik 1993 and references therein). For Seyfert galaxies, a substantial wind with $T_{\rm wind} \approx 1 \times 10^6$ K and $V_{\rm wind} \approx 200$ – 500 km s^{-1} is driven off if $L/L_{\rm Edd} \gtrsim 0.08$, where $L_{\rm Edd} \approx 3 \times 10^{12} (M_{\rm BH}/10^8 M_\odot)\ L_\odot$ the Eddington luminosity (e.g., Balsara & Krolik 1993). Unlike starburst-driven winds, Compton-heated AGN winds are directed along the minor axis of the *accretion* disk and are not necessarily perpendicular to the *galactic* disk.

Magnetic fields in accretion disks almost certainly play a critical role in powering and collimating AGN winds. Numerical simulations suggest that weakly magnetized accretion disks are subject to magnetorotational instability and inevitably produce magnetically active coronae (e.g., Miller & Stone 2000). The coronae likely generate outflows that are further boosted by centrifugal force (Blandford & Payne 1982; Königl & Kartje 1994). Hydromagnetically boosted outflows may be at the origin of the highly collimated, relativistic jets in powerful radio-loud galaxies (see reviews by Zensus 1997 and Worrall & Birkinshaw 2004). These narrow beams radiate inefficiently (Scheuer 1974), so most of their mechanical energy must heat and agitate the host ISM and the intracluster/intergalactic media (ICM/IGM). The scale over which the mechanical energy of the jets is deposited depends on several factors, including the distribution of ISM near the AGN, the jet power, and how collimated the outflow is at its source. Jets in radio-quiet systems are loosely collimated and barely relativistic (§5.2 and §5.3).

2.2 Wind-blown bubbles

Depositing mechanical energy by the starburst or the AGN over-pressurizes a cavity of hot gas in the starburst or near the AGN that reaches temperature

$$T = 0.4\ \mu m_H\ \dot{E}/k\dot{M}, \tag{7}$$

where $\dot{E}$ is the fraction of the mechanical energy injection rate that is thermalized and $\dot{M}$ is the rate at which the mass is heated. For a starburst, equation (7) can be re-written using equations (1) and (2) and assuming $\mu = 1.4$:

$$T \approx 3 \times 10^8\ \xi\ \Lambda^{-1}\ \ {\rm K}, \tag{8}$$

where ξ is the thermalization efficiency of the mechanical energy. The parameter Λ is the mass-loading factor, the ratio of the total mass of heated gas to the mass that is directly ejected by SNe and stellar winds or by the AGN. It accounts for the possibility that some of the ISM is mixed with the stellar or AGN ejecta. Note that this tenuous hot gas will be a poor X-ray (bremsstrahlung) emitter unless $\xi/\Lambda \ll 1$. The central pressure of the cavity is

$$P_o \approx 0.118\ \dot{E}^{\frac{1}{2}}\ \dot{M}^{\frac{1}{2}}\ R_*^{-2} = 0.08\ \dot{p}\ R_*^{-2}\ \ \text{dyne cm}^{-2}, \tag{9}$$

where R_* is the radius of the injection zone (Chevalier & Clegg 1985). R_* is the radius of the star-forming region in the case of a starburst-driven wind. We can rewrite equation (9) using equation (3) in this case:

$$P_o/k \sim 3 \times 10^5\ (SFR/M_\odot\ \text{yr}^{-1})(R_*/\text{kpc})^{-2}\ \ \text{K cm}^{-3}. \tag{10}$$

This pressure can significantly exceed the pressure of the undisturbed ISM, hence driving the bubble outflow. The hot cavity then evolves like a stellar wind-blown bubble, whose dynamics were analyzed by several authors (e.g., Castor, McCray, & Weaver 1975; Weaver et al. 1977; Ostriker & McKee 1988; Koo & Mckee 1992a,b). As hot gas expands through the sonic radius, it cools adiabatically (radiative cooling is small in comparison). Beyond the sonic radius, the wind drives a shock into the surrounding ISM and starts to sweep it into a shell of shocked gas. As the bubble boundary expands, the dense shell accumulates ISM and gradually slows the bubble's expansion to much less than the wind velocity. This marks the end of the adiabatic "free expansion" phase, whose duration is set by the mechanical luminosity of the starburst or AGN and the density of the ISM. At high mechanical luminosity ($\dot{E} > 10^{46}$ erg s^{-1}) and in gas-poor galaxies such as ellipticals ($n \sim 0.001 - 0.1$ cm^{-3}), free expansion may continue until the outer shock has traversed much of the host galaxy (e.g., Schiano 1985). In contrast, the free-wind phase in gas-rich starbursts and Seyfert galaxies is too short to observe.

Bubble evolution in gas-rich systems is described by the self-similar Taylor-Sedov solutions to a point-source explosion (blast wave) in a homogeneous medium (Taylor 1950; Sedov 1959). An extension by Schiano (1985) considered a continuous injection of wind energy in the Kompaneets approximation of an exponential atmosphere. After free expansion, the system develops an onion-like structure of five concentric zones; from smallest to largest radii there is (1) the energy injection zone where the mass and energy from the starburst or AGN is injected into the ISM, (2) a free-flowing, supersonic outflow immediately outside the injection zone, (3) a region of hot, shocked wind material, (4) a thin, dense shell of shocked ISM, and (5) undisturbed ISM. Note that the shocked ISM quickly becomes thermally unstable and collapses into a thin shell.

If radiative losses of the overall system are negligible, the expanding bubble is *energy-conserving*. In that case, the radius and velocity of the expanding shell of shocked ISM are given by (Castor et al. 1975; Weaver et al. 1977)

$$r_{\text{shell}} = 1.1\ (\xi \dot{E}_{44}/n_o)^{1/5}\ t_6^{3/5}\ \ \text{kpc}, \tag{11}$$

$$V_{\rm shell} = 640\ (\xi \dot{E}_{44}/n_o)^{1/5}\ t_6^{-2/5} = 670\ (\xi \dot{E}_{44}/n_o)^{1/3}\ r_{\rm shell,kpc}^{-2/3}\ \ {\rm km\ s^{-1}}, \quad (12)$$

$$(\xi \dot{E}) = 3 \times 10^{35}\ n_o\ r_{\rm shell,kpc}^2\ V_{\rm shell}^3\ \ {\rm erg\ s^{-1}}, \quad (13)$$

where t_6 is the age of the bubble in Myr, n_o is the ambient density in cm^{-3}, and $\dot{E}_{44}$ is the mechanical luminosity of the wind in units of 10^{44} erg s^{-1} (see, e.g., Shull & Saken 1995; Oey & Massey 1995; Oey 1996 for more general cases).

Momentum-conserving bubbles — where radiative losses are significant — decelerate faster: $r_{\rm shell} \propto t^{\frac{1}{2}}; V_{\rm shell} \propto t^{-\frac{1}{2}} \propto r_{\rm shell}^{-1}$ (e.g., Steigman, Strittmatter, & Williams 1975; Koo & McKee 1992a, 1992b). Their momentum injection rate is

$$\dot{p} \simeq 2 \times 10^{34}\ n_o\ r_{\rm shell,kpc}^2\ V_{\rm shell,100}^2 \quad {\rm dyne}. \quad (14)$$

2.3 Galactic winds

Once the shell has formed, if the wind-blown bubble approaches the scale height of the disk H, the shell reaccelerates, begins to fragment through growing Rayleigh-Taylor (RT) instabilities, and finally vents these fragments and the freely flowing and shocked wind into the galaxy halo. Energy-driven GWs (we discuss momentum-driven winds below) must be sufficiently energetic or long-lived to "breakout". Radiative losses in the wind must be mild enough not to drain too much energy from the wind to stall it; the cooling timescale must exceed the time for the bubble radius (Equation [11]) to reach $\sim H$. This occurs in the hot GW fluid (MacLow & McCray 1988), unless $\xi/\Lambda \ll 1$ (Equation [8]). The wind will break out if the expansion velocity of the shell (Equation [12]) near H exceeds the effective sound speed of the disk gas. The approximate criterion is

$$\xi \dot{E} \gtrsim 3 \times 10^{43}\ \ H_{\rm kpc}^2\ P_7^{3/2}\ n_o^{-\frac{1}{2}} \quad {\rm erg\ s^{-1}}, \quad (15)$$

where $H_{\rm kpc}$ is the disk scale height in kpc and P_7, the ambient pressure P/k in 10^7 K cm^{-3}, typical of starbursts (Schiano 1985; MacLow & McCray 1988; Norman & Ikeuchi 1989; MacLow, McCray, & Norman 1989; Koo & McKee 1992a; Strickland et al. 2004b).

The steady-flow wind is a strong function of polar angle seen from the starburst: The flow is a free wind up to the critical angle at which its ram pressure becomes comparable to the thermal pressure in the diffuse ISM. At larger angles, a standing bow shock in the galaxy disk decelerates and deflects the wind around undisturbed ISM. The terminal velocity of the wind can be estimated by equating the total energy deposition rate $\xi \dot{E}$ to the asymptotic rate of kinetic energy (KE) loss: $\frac{1}{2}\ \Lambda \dot{M} V_\infty^2 \approx \xi \dot{E}$. For a starburst-driven wind (eqns. 1 and 2) we obtain

$$V_\infty \approx (2\ \xi \dot{E}/\Lambda \dot{M})^{\frac{1}{2}} \approx 3000\ (\xi/\Lambda)^{\frac{1}{2}}\ \ {\rm km\ s^{-1}}. \quad (16)$$

The Λ dependence is easy to understand: cold ISM gas that feels the full brunt of the wind is shock heated and evaporated and eventually mass loads the hot flow, which slows the wind. Equation (16) assumes negligible halo drag.

Because momentum from the starburst or AGN cannot radiate away, a momentum-driven wind may exist even when most of the energy is gone. Then $\dot{p} = \Lambda \dot{M} V_\infty$,

where $\dot{p}$ is the sum of the radiation and mechanical momentum from the starburst or AGN. Outflow occurs if this exceeds the gravity of the host galaxy (e.g., Murray, Quataert, & Thompson 2005).

2.4 Hydrodynamical Simulations

The main impediment to understanding the dynamical evolution of GWs is that the bulk shocked wind is too hot to be studied by current X-ray observatories. Soft X-ray-emitting gas has been mapped (e.g. Fig. 2 & 3), but is of uncertain origin, seems to fill only a few percent of the volume, and contains at most 10% of the wind mass and energy. Simulations should therefore play a vital role in unraveling the dynamical evolution of this and other gas phases involved in the flow. However, gas at the shock velocities spanned by GWs ($\sim$ 20 to $\gtrsim$ 2000 km s^{-1}; §4.4) is unstable both dynamically and thermally: even several percent amplitude, pre-shock density fluctuations (Innes, Giddings, & Falle 1987a,b) are crushed by a 60-fold density increase while cooling to 10^4 K. Consequently, many computational cells are required to resolve cooling filaments and to track steep gradients. In fact, all but the most recent simulations have had to be two-dimensional, even though such axisymmetry closes "easy" dimensions to entropy flow and thereby forces disorder to emerge in inappropriate ways. Even simulations that adopted axisymmetry could handle only a limited range of gas densities. It was necessary to model separately the collision of the wind with low-density, diffuse ISM, and the collision with higher-density clouds found near the galaxy disk plane.

Axisymmetric simulations have explored a range of disk/halo values (e.g. Tomisaka & Ikeuchi 1988; Tomisaka & Bregman 1993), wind luminosities (e.g. MacLow & Ferrara 1999), mass loadings (Suchkov et al 1996; Hartquist, Dyson, & Williams 1997), metal versus mass-loss rates (especially in dwarf galaxies, e.g. MacLow & Ferrara 1999; D'Ercole & Brighenti 1999), and mass and energy deposition histories in the starburst (e.g. Strickland & Stevens 2000). Denser halos enhance emissivity, and are posited either from a larger dark matter load, or from high-latitude accretion debris that the wind may overrun. A disturbed, rarified, hot atmosphere from previous outbursts has been incorporated into some AGN jet simulations (e.g. Smith et al. 1983), but not yet for starburst winds.

After the wind impacts a dense cloud, (Klein, McKee, & Colella 1994; Silich et al. 1996; Hartquist, Dyson, Williams 1997; Poludnenko, Frank, & Blackman 2002; Williams & Dyson 2002), subsonic flow at the apex becomes transonic around the cloud edges, inducing Kelvin-Helmholtz (KH) instabilities. Clouds therefore soon develop a core/structured halo. Filaments in the halo disappear by photo- or thermal-evaporation before moving far from the core. Schiano, Christiansen, & Knerr (1995, also Vietri, Ferrara, & Miniati 1997) show that the halo penetrates only to the depth of the KH instabilities. The halo ablates from the unscathed core, dumping the entropy induced by the enveloping shocked wind in a series of "shedding events" that "fire polish" the cloud surface to reset the KH clock. By ablating small bumps, the cloud core stabilizes itself against disruptive larger instabilities and can survive to accelerate toward the wind speed.

In more energetic outflows into a denser ISM, mass loading can cause RT instabilities to culminate in repeated, large vortices that crush gas along shocks as the bubble apex shreds. Elsewhere the wind flow can be almost adiabatic, progressing so rapidly that the timescales for recombination, collisional ionization, and excitation exceed greatly the dynamical time (Breitschwerdt & Schmutzler 1999). The gas soon becomes very convoluted, with a fractal size distribution that Sutherland, Bicknell, & Dopita (2003a) show enhances cooling, hence shock prominence, compared to steady-flow models.

Steady winds can develop a "stagnation ring shock" in the disk plane. Tenorio-Tagle & Muñoz-Tuñón (1997, 1998) show how this shock becomes prominent when the ram pressure of even diffuse H I augments the thermal pressure of the enveloping gas. Wind fueling stalls the ring at constant radius, a result consistent with the sparse kinematical data on ring shocks (§4.3). Feedback occurs because the base of the wind controls the minimum mass accreted for the starburst to maintain the wind, but computer limitations have thus far prevented coupling of starburst and hydrodynamical codes of useful resolution.

In fact, most winds fail to develop a large-scale, steady flow. The small free-wind zone is then bounded at smallest radius by a few cells of energy injection at the base, and at largest radius by the boundary between dense clouds and their upstream bow shocks that appear as elaborate filamentation at the resolution imposed by the grid. Figures 2 and 3 show that the boundary emits most of the soft X rays. Figure 1 is an example of a recent three-dimensional simulation that, by detailing this region, promises to pin down the elusive X-ray filling factor.

3 MAJOR WINDBLOWN EVENTS IN THE LMC & GALAXY

The Galaxy and the Large Magellanic Cloud are excellent laboratories for detailed studies of wind-blown events. The processes involved in these local events are scaled down versions of superbubbles and GWs in starburst galaxies. We summarize key features of these local laboratories in this section.

3.1 Large Magellanic Cloud

The largest H II region in the LMC (and indeed Local Group), 30 Doradus, is a microcosm of starburst processes. Cluster R136 powers the nested shells and superbubbles. This mini-starburst contains ∼50 very massive stars and has an estimated initial mass of a few 10^4 $M_\odot$ (Malamuth & Heap 1994; Brandl et al. 1996; Brandl 2005). For comparison, M82 is powered by the equivalent of ∼ 100 R136's within a region only 2-3 times larger than 30 Dor (Rieke et al. 1980; Muxlow et al. 1994; O'Connell et al. 1995). Shells and compact knots moving at ∼ 200 km s^{-1} are detected in 30 Dor (Chu & Kennicutt 1994; Redman et al. 2003), perhaps forming the base of a large-scale wind able to escape the LMC ($v_{\rm esc} \approx 150$ km s^{-1}). Many shells in 30 Dor seem to be momentum-conserving, not pressure-driven.

3.2 Nuclear Wind in the Galaxy

Only 8.0±0.5 kpc (Reid 1993) distant, the Galactic Center shows remarkable energetic activity at infrared (IR), radio, X-ray and γ-ray wavelengths (Morris & Serabyn 1996; Yusef-Zadeh et al. 2000, 2005; Cheng et al. 1997). While this activity has proved difficult to disentangle, there is now solid evidence on scales of arcminutes to tens of degrees for powerful mass ejections from the Galactic Center. The idea of a central explosion dates back to the early discovery of peculiar H I kinematics there (see §1.1), but we know today that most, but not all, of the H I kinematical signature is due to streaming motions arising from a central bar (Morris & Serabyn 1996).

A particular problem with GW studies has been deriving reliable energies from multi-wavelength observations at comparable resolution. Current estimates of the energetics of our Galactic Center span a huge range. Sofue & Handa (1984) discovered the 200 pc diameter Galactic Center radio lobe (GCL; Fig. 2*b*), with an implied thermal energy of $\sim 3 \times 10^{51}$ erg. Chevalier (1992) argued for a higher value ($\sim 2 \times 10^{52}$ erg) due to winds from hot young stars over the past 30 Myr. Others have argued from the high temperatures implied by the ASCA detection of 6.7 keV Kα emission from He-like Fe XXV (Koyama et al. 1989, 1996; Yamauchi et al. 1990; but see Wang, Gotthelf, & Lang 2002) that an explosive event ($4 - 8 \times 10^{53}$ erg) must have occurred. Bland-Hawthorn & Cohen (2003) detected the GCL at mid-IR wavelengths (Fig. 2*b*). The association of the lobe with denser material raises the energetics to $10^{54}/\kappa$ erg, where κ is the covering fraction of the dense shell; less energy is needed if there is substantial polycyclic aromatic hydrocarbon (PAH) emission with the mid-IR continuum. These energetics assume a shell velocity of ~ 150 km s^{-1}, a value based on the kinematics of the neighboring molecular gas after correction for bar streaming (Bally et al. 1988); this value is uncertain because of our location in the plane. The ROSAT 1.5 keV diffuse X-ray map over the inner 45° provides compelling evidence for this GW interpretation (Fig. 2*a*) (Bland-Hawthorn & Cohen 2003). Evidence for outflows on smaller scale may be present in *Chandra X-ray Observatory* (CXO) X-ray maps (Baganoff et al. 2003).

Potential energy sources are young star clusters or the $3 - 4 \times 10^6$ M$_\odot$ central BH (Oort 1977; Frogel 1988; Genzel et al. 1996; Schödel et al. 2003; Ghez et al. 1998, 2005). Individual star clusters have ages ranging from 5 Myr (Krabbe et al. 1995) to 20 Myr (Eckart, Ott, & Genzel 1999; Figer et al. 2000). While the star formation history is undoubtedly complicated, there is now abundant evidence that the Galactic Center has experienced several starburst episodes (e.g., Tamblyn & Rieke 1993; Sjouwerman et al. 1998; Simpson et al. 1999). Detailed models of PAH and fine structure features (Lutz 1998) suggest a starburst ∼7 Myr ago, supported by a census of stars (Genzel et al. 1994; Krabbe et al. 1995; Najarro et al. 1997).

Activity seems to be fueled from the central molecular zone (CMZ), a "ring" at 180 pc radius with M$_{\rm cmz} \sim 8 \times 10^6$ M$_\odot$. Inflow rates of ~ 1 M$_\odot$ yr^{-1} to the Galactic Center (Morris & Serabyn 1996) suffice to trigger starbursts and nuclear

activity in Seyfert galaxies ($\sim 10^{43}$ erg s^{-1}). Hydro simulations (§2.4) show that a central explosion of $\sim 10^{55-56}$ erg would provide mass M_{cmz} with sufficient radial impulse to make the observed ring (Sanders 1989; Saito 1990).

4 LOCAL CENSUS OF GALACTIC WINDS IN STAR-FORMING GALAXIES

In the next two sections, we present a census of galactic winds. Each newly discovered outflow source provides different insights into the wind process, and often reveals new and complex behavior. Therefore, it is necessary to summarize what is known of the wind phenomenon in terms of basic observational parameters (e.g. morphology, kinematics, energetics). The subject of galactic winds is largely in its infancy; therefore a discussion of the phenomenology is warranted here. We start by summarising the search techniques used to find outflow sources, the limitations of each technique and the inferred detection rates.

4.1 Search Techniques & Observational Limitations

The wind phenomenon is likely to be sufficiently complex that a multiwavelength approach is necessary in order to probe all gas phases. Line and continuum emission from warm, hot, and relativistic plasma have been used with great success to identify or confirm GWs. Choice emission lines are Hα, [N II] $\lambda\lambda$6548, 6583, [S II] λ6716, 6731, [O III] λ5007, and [O II] λ3727 in the optical, and Paα, Brγ, and H_2 2.122 μm in the near-IR. Lyα λ1216 should be avoided because resonant scattering and selective dust absorption severely distort its emission profile and intensity (e.g., Tenorio-Tagle et al. 1999; Keel 2005). CXO and the XMM-Newton Observatory have provided powerful new tools for complementary searches in soft X rays, whereas facilities such as the upgraded *Very Large Array* (VLA) will continue efficient radio studies of winds.

Enhanced emission along the minor axis of the host galaxy does not necessarily imply a GW; other origins include tidal interaction and ram-pressure stripping by the ICM. Kinematic signatures of extraplanar, non-gravitational effects are needed to be certain. Double-peaked emission-line profiles attributable to an expanding, shocked shell are often evident in wind galaxies. Emission-line ratios typical of shock excitation (e.g., [N II] λ6583/H$\alpha \geq 1$; [S II] $\lambda\lambda$6716, 6731/H$\alpha \geq 0.5$) indicate winds, but these diagnostics favor powerful ones with large outflow velocities and a weak starburst radiation field (see §4.8 for more detail).

Selection effects hamper detection of GWs: "Since deceleration is what powers all of the emission process, the brightness distribution due to a particular emission process will be dominated by the sites of optimum local deceleration (corresponding to an optical density and temperature contrast) within the range of decelerations that can give rise to that process" (Braun 1985). Observable winds are likely those that are only slightly more pressured than the galaxy potential. Highly energetic winds ($\gg 10^{58}$ erg or $\gg 10^{44}$ erg s^{-1} from Equation [15]) may escape undetected, although this will depend on such details as how

energy is injected at the source, and the amount of gas in and around the host galaxy. Winds $\ll 10^{41}$ erg s^{-1} would have little observable impact on the ISM of an external galaxy.

The need to distinguish wind-related emission from the background favors detection of highly inclined outflows in edge-on galaxies. This is true for most of the well-known starburst-driven winds. In a few less inclined galaxies (e.g., NGC 253, NGC 1808), outflows were first suspected on the basis of absorbing dust filaments seen against the galaxy body (e.g., Phillips 1993). In NGC 253, extended Hα filaments are projected onto disk H II regions, requiring detailed 3D kinematics to separate the different components. Similar blending occurs at X-ray and radio wavelengths because compact sources are commonly associated with the inner disk. In edge-on systems, kinematical deprojection leads to large uncertainties in wind energetics. Other complications include uncertain dereddening at the base of the outflow, relating the post-shock to the pre-shock velocities, and high density bias introduced by the density-squared dependence of the emission measure.

Absorption-line techniques have been used with great success to search for the unambiguous wind signature of blueshifted absorbing material in front of the continuum source. This method favors detection of winds in face-on systems and therefore complements the emission technique. The equivalent width and profile of the absorption line are used to estimate the amount of outflowing material along the line of sight and to determine its projected kinematics. For an unsaturated line, the column density of the absorbing material scales linearly with the equivalent width of the line and therefore is arguably a better probe of the whole range of density in the wind than the line or continuum emission. For saturated lines, the change in equivalent width reflects primarily a change in the velocity dispersion of the absorbing clouds, covering fraction or both.

UV interstellar absorption lines are useful. Low-ionization lines such as Si II λ1260, O I + Si II λ1303, C II λ1334, Si II λ1526, Fe II λ1608, and Al II λ1670 are particularly well suited to avoid confusion with possible stellar photospheric features of higher ionization (e.g., C III λ1176, O IV λ1343, S V λ1501) and stellar wind features with P Cygni-type profiles (e.g., N V $\lambda\lambda$1238, 1242, Si IV $\lambda\lambda$1393, 1402, C IV $\lambda\lambda$1548, 1550, He II λ1640). A few key optical lines have also been used in successful wind searches in $z \lesssim 0.5$ galaxies: Na I D $\lambda\lambda$5890, 5896 and K I $\lambda\lambda$7665, 7699. Extension to the far-UV domain with the *Far Ultraviolet Spectroscopic Explorer* (FUSE) spacecraft has recently allowed the use of the OVI $\lambda\lambda$1032, 1038 lines to probe the coronal-phase (T = a few $\times$ 10^5 K) gas in GWs. Such measurements constrain the amount of radiative cooling (see §4.5).

4.2 Detection Rate

There are now estimates of the frequency of wind occurrence in nearby star-forming galaxies for most wavebands. Detailed studies of extended optical line emission around various starburst and quiescent galaxies reveal a clear trend between starburst strength and the presence of kinematically confirmed winds

or extraplanar diffuse ionized gas (e.g., Heckman, Armus, & Miley 1990; Hunter, Hawley, & Gallagher 1993; Pildis, Bregman, & Schombert 1994; Lehnert & Heckman 1995, 1996; Marlowe et al. 1995; Veilleux et al. 1995; Rand 1996; Hunter & Gallagher 1997; Kim, Veilleux, & Sanders 1998; Martin 1998; Miller & Veilleux 2003a, 2003b; Rossa & Dettmar 2000, 2003a, 2003b; although see Meurer 2004). Complementary results from systematic searches for blueshifted optical absorption lines (e.g., Heckman et al. 2000; Rupke, Veilleux, & Sanders 2002, 2005a, 2005b; Schwartz & Martin 2004; Martin 2005), complex UV emission and absorption lines (e.g., Lequeux et al. 1995; Kunth et al. 1998; Heckman et al. 1998; Gonzalez Delgado et al. 1998), extended emission in soft X rays (e.g., Read, Ponman, & Strickland 1997; Dahlem, Weaver, & Heckman 1998; Pietsch et al. 2000; McDowell et al. 2003; Ehle et al. 2004; Huo et al. 2004; Strickland et al. 2004a, 2004b; Ehle 2005; Grimes et al. 2005) and at radio wavelengths (e.g., Hummel, Beck, & Dettmar 1991; Irwin, English, & Sorathia 1999; Irwin, Saikia, & English 2000; Dahlem et al. 2001) all confirm this dependence on starburst strength.

A key indicator is 60-to-100 μm IRAS color, S_{60}/S_{100}, which tracks dust temperature in star-forming regions. "Warm" 60-to-100 μm IRAS color — $S_{60}/S_{100} \gtrsim 0.4$ — is often used to classify galaxies as starbursts. Warm galaxies generally have large IR luminosities ($\gtrsim 10^{10.5}$ L$_\odot$), excesses (L$_{\rm IR}$/L$_{\rm opt}$ $\gtrsim 2$), and galaxy-averaged far-IR (FIR) surface brightnesses (L$_{\rm FIR}/\pi R_{25}^2 \gtrsim 2 \times 10^{40}$ erg s^{-1} kpc^{-2}; e.g., Rossa & Dettmar 2003a). This is not surprising because the SFR scales with the IR luminosity according to equation (5), and the dust temperature is expected to scale with the UV energy density. The conditions on the IR luminosity and surface brightness in warm galaxies translate into SFR $\gtrsim 5$ M$_\odot$ yr^{-1} and SFR$/\pi R_{25}^2 > 0.001$ M$_\odot$ yr^{-1} kpc^{-2}. Almost all of these galaxies have extraplanar ionized gas, and most also host a wind. More than 75% of ultraluminous IR galaxies (ULIRGs) with IR luminosities $> 10^{12}$ L$_\odot$ ($S_{60}/S_{100} \gtrsim 0.5$) have winds (e.g., Rupke et al. 2002, 2005b; Martin 2005). The degree of nucleation of star formation activity increases with SFR, so it is not surprising to detect so many winds among ULIRGs (where SFR $\gtrsim 100$ M$_\odot$ yr^{-1} and $R_* < 1$ kpc).

4.3 Morphology

The outflows in most star-forming galaxies have a bipolar distribution perpendicular to the disk. Opening angles are $2\theta \approx 10^\circ - 45^\circ$ near the base, increasing to $\sim 45^\circ$ – 100° above the disk as expected from simulations (§2.4). But the detailed gas distribution is often complex, shows large galaxy-to-galaxy variations, and depends on the specific gas phase. In optical line emission, outflow structures range from the classic egg-shaped nuclear superbubble of NGC 3079[1] (Fig. 3; Ford et al. 1986; Veilleux et al. 1994; Cecil et al. 2001) to the bipolar double-loop morphology of Arp 220 (Heckman, Armus, & Miley 1987), the bicon-

[1]NGC 3079 has both a nuclear starburst and an AGN, but from the morphology and kinematics of the line emitting gas, Cecil et al. (2001) conclude that this outflow is starburst, not AGN, powered.

ical structure of M82 (Fig. 4; Bland & Tully 1988; Shopbell & Bland-Hawthorn 1998; Ohyama et al. 2002) and NGC 1482 (Fig. 5*a*; Veilleux & Rupke 2002), and the frothy and filamentary morphology of the outflow in the dwarf NGC 1569 (e.g., Martin, Kobulnicky, & Heckman 2002). The line-emitting structures are often limb-brightened, indicating that much of the optically emitting gas resides on the surface of largely hollow structures. In the few objects examined with the *Hubble Space Telescope* (HST) ($\sim 0\farcs1$), the line-emitting gas is resolved into complexes of clumps and filaments (e.g., M82) or streams of filamentary strands and droplets (e.g., NGC 3079) with volume filling factors $f \gtrsim 10^{-3}$. The morphology and kinematics (discussed in §4.4) of this gas suggest that it originated in the cool disk and became entrained in the outflow.

These structures vary in vertical extent from ~ 1 kpc to $\gtrsim 20$ kpc (see Veilleux et al. 2003 and references therein). Large filaments seemingly unrelated to the nuclear structure sometimes appear in deeper exposures; e.g., faint X-shaped filaments extend > 8 kpc from the nucleus of NGC 3079 (Heckman et al. 1990; Veilleux et al. 1994) and rise ~ 4 kpc from the galactic plane but connect to the inner ($R \approx 1.5$ kpc) galactic disk rather than to the nucleus itself. Cecil et al. (2001) suggest that these filaments have the shape expected (Schiano 1985) for the contact discontinuity/ISM associated with lateral stagnation of the wind in the galaxy thick disk/halo. The lateral extent of the wind is necessarily much smaller in the disk, where one expects to find a "ring shock." This feature (see §2.4) has been detected in a few objects, based on line emission and warm molecular gas emission (e.g., NGC 253: Sugai, Davies, & Ward 2003; see below).

A growing set of $\sim 1''$-resolution CXO data show that the bright, soft X ray and Hα filaments in these winds have strikingly similar patterns on both small and large scales ($\sim 0.01 - 10$ kpc; e.g., Strickland et al. 2000, 2002; Cecil, Bland-Hawthorn, & Veilleux 2002a; McDowell et al. 2003; Strickland et al. 2004a). This tight optical-line/X-ray match seems to arise from cool disk gas that has been driven by the wind, with X rays being emitted from upstream, standoff bow shocks or by conductive cooling at the cloud/wind interfaces. This is not always the case for the fainter soft X-ray emission. For instance, the X-ray emission near the X-shaped filaments of NGC 3079 (Fig. 3*a*) is not significantly edge brightened, suggesting a partially filled volume of warm gas within the shocked wind, not a shell of conductively heated gas (Cecil, Bland-Hawthorn, & Veilleux 2002; see also Huo et al. 2004; Ott, Walter, & Brinks 2005). In a few objects, absorption by foreground neutral ISM also affects the distribution of the soft X-ray emission (e.g., NGC 253: Strickland et al. 2000; M82: Stevens, Read, & Bravo-Guerrero 2003). Intrinsically hard, diffuse X-ray emission has been detected in a few wind galaxies. In M82, this gas is more nucleated but less filamentary than the soft X-ray emission; it probably traces the hot, high-pressure wind fluid (Griffiths et al. 2000; Stevens et al. 2003; see §4.9 for more detail).

Several wind galaxies have large radio halos (e.g., M82: $Z \approx 5$ kpc, Seaquist & Odegard 1991; NGC 253: ~ 9 kpc, Carilli et al. 1992; NGC 3079: ~ 11 kpc, Irwin & Saikia 2003; NGC 4631: ~ 9 kpc, Hummel & Dettmar 1990). Galaxies with thick ionized disks ($S_{60}/S_{100} > 0.4$) also tend to show extrapla-

nar synchrotron radio emission (e.g., Dahlem et al. 2001). Given the significant polarization of the radio emission and the lack of point-by-point correspondence with the X-ray and optical line emission, non-thermal synchrotron from magnetized ($B \approx$ few $\times 10\mu$G), relativistic electrons is the favored explanation for most of the radio emission. The pattern of magnetic field lines in NGC 3079 (Cecil et al. 2001) suggests that the relativistic electrons are produced in the starbursting disk and then advected from the disk by the wind. Some emission may also come from electrons accelerated locally in internal wind shocks. Steepening of the spectral index of the radio continuum emission in M82 (Seaquist & Odegard 1991), NGC 253 (Carilli et al. 1992), NGC 4631 (Ekers & Sancisi 1977; Hummel 1991) and NGC 891 (Allen, Sancisi, & Baldwin 1978; Hummel 1991) indicates energy losses of the electrons on their way from the starburst, either from synchrotron losses or inverse Compton scattering of the relativistic electrons against the IR photons produced in the nuclear region. In some objects, the relativistic component of the wind appears to decouple from the thermal component beyond the Hα-emitting structures (e.g., NGC 3079, Duric & Seaquist 1988), perhaps participating in a "cosmic ray wind" rather than a thermal wind (Breitschwerdt & Schmutzler 1999).

Unambiguous evidence for entrained neutral gas has been detected from dwarf galaxies (e.g., Puche et al. 1992; Stewart et al. 2000; Schwartz & Martin 2004) to ULIRGs (e.g., Heckman et al. 2000; Rupke et al. 2002, 2005a, 2005b; Martin 2005). This gas often extends up to several kiloparsec, but morphological constraints are sparse. Detailed long-slit spectra show some degree of correlation with the warm ionized gas (§4.4). Kinematically disturbed molecular gas has also been detected in a few GWs. The best case for molecular gas entrained in a GW is in M82, where a detailed kinematical decomposition of the CO gas into wind and disk components reveals a wide-angle (opening angle $2\theta \approx 110^\circ$) pattern related loosely to the outflow seen at other wavelengths (Stark & Carlson 1984; Seaquist & Clark 2001; Walter, Weiss, & Scoville 2002). A narrow, shock-excited SiO chimney extends ~ 500 pc above the disk (Garcia-Burillo et al. 2001), and is also found in NGC 253 (Garcia-Burillo et al. 2000). Shocked H_2 gas is detected at the base of the outflow of NGC 253 (Sugai et al. 2003), consistent with the cloud-crushing model of Cowie, McKee, & Ostriker (1981) and Ohyama, Yoshida, & Takata (2003) where C-type shocks with $V_{\rm shock} \lesssim 40$ km s^{-1} are compressing the star-forming molecular disk.

GW structures sometimes tilt relative to the minor axis of the host, and are asymmetric to the nucleus. Tilts and asymmetries near the starbursts (M82: Shopbell & Bland-Hawthorn 1998; Galaxy: Bland-Hawthorn & Cohen 2003; NGC 253: Sugai et al. 2003) probably reflect asymmetries in the starbursting population and in the density distribution of the cool, star-forming disk. Asymmetries on large scales may be due to density fluctuations in the halo of the host galaxy, and therefore can be a probe. The IGM through which the galaxy is moving may also influence the morphology of the wind structure on large scales (e.g., radio halo in M82, Seaquist & Odegard 1991).

4.4 Kinematics

Spectra of the warm ionized component in GWs shows double-peaked emission-line profiles with a split ranging from a few 10's of km s^{-1} in some dwarf galaxies (e.g., Marlowe et al. 1995; Martin 1998) to nearly 1500 km s^{-1} in NGC 3079 (Filippenko & Sargent 1992; Veilleux et al. 1994). Constraints on the phase-space distribution of gas within the outflows are necessary to deproject observed velocities. The dense 2D spatial coverage of Fabry–Perot and IF spectrometers is ideal, but usually only narrow-band imaging and long-slit spectroscopy are available to constrain the outflow geometry. The observed kinematic patterns indicate that most warm gas lies on the surface of expanding bubbles/ellipsoids or flows along the walls of conical structures. The substantial broadening often seen in individual kinematic components indicates that the flow is not purely laminar or that the cone walls are composites of distinct filaments with a range of velocities.

The most detailed studies of outflow kinematics can be compared quantitatively with the hydro simulations described in §2.4. The deprojected outflow velocity in open-ended conical winds often increases with radius as expected for entrained gas in a free-flowing wind (e.g., Murray et al. 2005); examples are M82 (Shopbell & Bland-Hawthorn 1998) and NGC 3079. Gas near the top of the partially ruptured bubble of NGC 3079 is entrained in a mushroom vortex (Cecil et al. 2001), as predicted theoretically (e.g., Suchkov et al. 1994). In these open-ended winds, there is a clear correlation between outflow velocity and gas phase temperature. For example, cool molecular gas is ejected out of M82 at a maximum deprojected outflow velocity of $\sim$ 230 km s^{-1} (Shen & Lo 1995; Walter et al. 2002), well below the inferred velocities of the warm ionized gas (525 – 655 km s^{-1}; Shopbell & Bland-Hawthorn 1998). Coronal gas traced by the O VI λ1032 absorption line in NGC 1705 is more blueshifted than the neutral gas, whereas the warm photoionized gas appears to have intermediate velocities (Heckman et al. 2001a). Smaller outflow velocities in the neutral gas relative to the ionized components are also often seen in LIRGs and ULIRGs (Rupke et al. 2005b). These systematic kinematic variations with phase temperature are consistent with entrainment of gas clouds by a hot wind if the warmer phase has smaller column densities than the cool gas, perhaps as a result of cloud erosion (§2.4).

Entrainment of disk material is supported by other evidence, including the detection of rotation in the outflow gas (e.g., M82: Shopbell & Bland-Hawthorn 1998, Greve 2004; NGC 3079: Veilleux et al. 1994; NGC 1482: Veilleux & Rupke 2002) and the field reversal across the NGC 3079 radio lobe that suggests the return of entrained, magnetized material to the disk (Cecil et al. 2001).

Wind kinematics are poorly constrained. This fluid, being hot and tenuous (§4.9 and Equation [8]), is hard to detect, so current X-ray instruments do not constrain its velocity. A lower limit follows from the expected terminal velocity of an adiabatic wind at the measured X-ray temperature T_X: $V_W^2 \simeq \alpha\ c_s^2 = \alpha\ kT_X/\mu m_p$, where c_s is the isothermal sound speed of the hot phase, μm_p, the mean mass per particle, and $\alpha = 2.5 - 5.0$, a scale factor that depends on the

fraction of thermal energy that is radiated (e.g., Appendix B in Efstathiou 2000). This is a lower bound because it accounts only for thermal energy and neglects possibly substantial (e.g., Strickland & Stevens 2000) bulk motion. Measured X-ray temperatures in GWs are quite uniform ($\sim 0.2 - 2 \times 10^7$ K; Martin 1999; Heckman et al. 2000; Strickland et al. 2004a), and imply $V_W \simeq 500 - 900$ km s^{-1}. These are well below V_∞ from equation (16) unless $\xi/\Lambda \ll 1$. Note that the X-ray temperature is weighted by the emission measure, so it probes only dense shocked material between disk and wind gas. The measured X-ray temperature is therefore likely a *lower* limit to the wind temperature, and wind velocities are also lower limits.

Our knowledge of the kinematics of neutral gas in GWs has improved considerably thanks to Na I D absorption-line surveys (e.g., Heckman et al. 2000; Rupke et al. 2002, 2005a, 2005b; Schwartz & Martin 2004; Martin 2005). The profile of the interstellar Na I absorption feature is fit with multiple components to determine the bulk and turbulent velocities of the neutral gas. The resulting distribution of Na I D velocities is skewed to the blue (relative to systemic); this is interpreted as outflow. Line full widths at half maximum (FWHMs) average $\sim$ 275 km s^{-1} in large starbursts, much larger than the thermal velocity dispersion of warm neutral gas. This broadening comes from the superposition of distinct kinematic components with several radial velocities, as seen in the warm gas phase. The projected "maximum" velocities in the outflowing components (equal to the centroid velocity plus one-half the velocity width) average 300 – 400 km s^{-1}, and attain $\sim$ 600 km s^{-1} (although 1100 km s^{-1} is seen in F10378+1108). Figure 6*a* plots the maximum outflow velocities against host-galaxy mass. A linear least-squares fit suggests that outflow and circular velocities correlate positively, but this correlation is mainly due to the dwarf galaxies (Rupke et al. 2005b, Martin 2005).

Figure 6*b* compares the outflow velocities with the host galaxy SFR ($L_{\rm IR}$). There is some indication of a trend of increasing outflow velocities with increasing SFR, particularly when data from Schwartz & Martin (2004) on dwarf galaxies are included. Figure 6*b* shows that cloud entrainment in a wind (Equation [A5] in Murray et al. 2005) is able to reproduce these velocities, except perhaps for F10378+1108 where the large outflow velocity may also require radiation pressure. (Martin 2005 has also argued for radiation-pressure driving in other objects). UV absorption-line measurements appear to confirm the positive correlation between outflow velocities and SFR's (Heckman 2004).

4.5 Mass Outflow Rates & Energetics

The multiphase nature of GWs greatly complicates the task of estimating the outflow masses and energies. A multiwavelength approach that considers all phases is essential. Given the density-squared dependence of the emission measure, diagnostics that rely on line or continuum emission favor the densest material, yet this may be only a relatively small fraction of the total mass and energy. This is especially relevant for the wind fluid, which is expected to dominate the energetics

of the outflow, but contributes very little to the emission (Strickland & Stevens 2000). Corrections must be applied for the volume filling factor, f. Constraints on f can be derived from estimates on the volume of the emitting material and assumptions about its emissivity (temperature). Measurements that rely on absorbing column densities are less subject to density inhomogeneities, but require a strong source of background light and therefore are limited to the brightest parts of the starburst. Assumptions about filling factor and outflow extent must then be made to estimate the mass of outflowing material and the energetics.

After deprojecting observed velocities, the dynamical timescales of starburst-driven outflows ($t_{\rm dyn} \approx R/V_{\rm out}$) range from 0.1 to 10 Myr. The mass of warm ionized gas inferred to take part in the outflow is $\sim 10^5$ – 10^6 $M_\odot$ in dwarf galaxies and $\sim 10^5$ – 10^7 $M_\odot$ in powerful starbursts. The dynamical timescales yield mass outflow rates ranging from $\lesssim 0.1$ $M_\odot$ yr^{-1} to $\gtrsim 10$ $M_\odot$ yr^{-1}, with a trend for the rate to increase with increasing SFR. A similar trend may exist between star formation activity and the amount of extraplanar gas in non-starburst galaxies (e.g., Dettmar 1992; Rand, Kulkarni, & Hester 1992; Miller & Veilleux 2003a; Rossa & Dettmar 2003a).

Bulk plus "turbulent" KEs inferred from optical emission-line spectra span a broad range: e.g., NGC 1482: $\gtrsim 2\times10^{53}$ erg (Veilleux & Rupke 2002); NGC 3079: $\sim 10^{54}$ erg (Cecil et al. 2001); M82: $\sim 2\times10^{55}$ erg (Shopbell & Bland-Hawthorn 1998). These are typically several times lower than thermal energies derived from X-ray data. Luminosities of galactic X-ray halos scale roughly with IR luminosities or disk SFRs (Strickland et al. 2004a, 2004b), but the corresponding X-ray cooling rates amount to $\lesssim 10\%$ of the SN heating rates in these objects. Cooling by the optical line-emitting material is even smaller.

Results from Na I D studies suggest that GWs entrain considerable neutral material, $\sim 10^4-10^7$ $M_\odot$ (0.001 – 1.0 $M_\odot$ yr^{-1}) in dwarfs and $\sim 10^8-10^{10}$ $M_\odot$ ($\sim$ 10 – 1000 $M_\odot$ yr^{-1}) in ULIRGs. These rates generally exceed the mass injection rate from SNe (Equation [1]). However, they are highly uncertain because: (1) the geometry of the neutral outflow is poorly known (here the simple model of a mass-conserving free wind from Rupke et al. 2005b is used with the assumption that gas lies in a thin shell at a radius ~ 5 kpc for the large starbursts; and at smaller radii for the dwarfs; the estimated masses scale linearly with this radius); (2) depletion of Na onto grains affects the strength of the Na I D absorption line (here we assume a depletion factor ~ 9); (3) the ionization potential of Na is low (5.139 eV) so considerable Na is ionized even when hydrogen is neutral; this must be accounted for when calculating H^0 masses (the ionization correction is assumed to be close to the Galactic value of ~ 10).

Assuming that these estimates of neutral gas masses are correct, the ratios of $\dot{M}$ to the global SFRs span $\eta \equiv \dot{M}/{\rm SFR} \approx 0.01-10$, consistent with those found by Martin (1999) for the warm ionized medium of ten galaxies. Parameter η, the mass entrainment efficiency, shows no obvious dependence on SFR except perhaps at high SFR where $\eta \sim 0.1$. The inferred KE increases with increasing SFR: $\sim 10^{50}-10^{54}$ erg among dwarfs but $\sim 10^{56}-10^{59}$ erg among LIRGs and ULIRGs; corresponding power outputs are $\sim 10^{36}-10^{39}$ and $10^{41}-10^{44}$ erg s^{-1},

respectively. Such energies and powers exceed those of the outflowing warm ionized gas. Contrary to some expectations (e.g., Silk 2003), the trend with SFR flattens among ULIRGs, perhaps due to the complete evacuation of the gas in the wind's path, a common neutral gas terminal velocity for LIRGs and ULIRGs, and/or a decrease in the efficiency of thermalization of the SN energy.

CO studies of GWs are very important because so much mass is required to see molecular gas that its detection dramatically increases the inferred energies. A good illustration is M82: Walter et al. (2002) deduced from CO observations that $> 3\times\ 10^8$ $M_\odot$ of H_2 is involved in the outflow, and its KE $\sim 10^{55}$ erg becomes comparable to the KE in the warm filaments. We discussed in §3.2 the GW of the Milky Way, where cold material seems to dominate the KE of the outflow. Detailed millimeter studies of a representative set of GWs will be needed to confirm the dynamical importance of the molecular gas component.

The latest addition to the mass and energy budgets of GWs is the coronal ($T \sim 10^5$ K) phase traced by O VI. Dynamical information on this component is currently sketchy, outflowing gas being detected in absorption in only two (dwarf) galaxies so far: NGC 1705 ($v_{\rm out} \approx 100$ km s^{-1}; Sahu & Blades 1997; Heckman & Leitherer 1997; Heckman et al. 2001) and NGC 625 ($v_{\rm out} \approx 30$ km s^{-1}; Cannon et al. 2005). The mass of coronal gas derived from these data is uncertain because of possible line saturation, ionization corrections, and assumptions on the gas geometry. In NGC 1569, Heckman et al. (2001a) estimate a mass of $\sim 6 \times 10^5$ $M_\odot$ and KE of $\sim 3 \times 10^{52}$ erg in the coronal phase. These are only $\sim 1\%$ of the values in the warm ionized phase, so the coronal component is unimportant dynamically. But what about its radiative losses? The O VI $\lambda\lambda$1032, 1038 lines are key because they produce $\sim 30\%$ of the coronal cooling. O VI emission was detected in NGC 4631 (Otte et al. 2003), but not in NGC 1705 (Heckman et al. 2001a), M82 (Hoopes et al. 2003), and NGC 891 (Otte et al. 2003). These measurements limit the radiative cooling of coronal gas to 10 – 20% of the SN heating rate in these objects. To within a factor of 2, this is identical to the cooling rate of the X-ray-emitting gas.

4.6 Escape Fraction

The fraction of outflowing material that can escape the gravitational potential of the host galaxy is an important quantity but is difficult to determine accurately. It should be recalled that within the context of CDM theory, the virial radius of the dark halo is $\sim 250 h_{70}^{-1}$ kpc for an L_* galaxy, with the IGM beyond.

Can winds reach the IGM? The main uncertainty comes from our lack of constraints on halo drag. Silich & Tenorio-Tagle (2001) have argued that drag may severely restrict a wind and limit its escape fraction. Drag by a dense halo or tidal debris may be especially important in high-luminosity starbursts because many are triggered by galaxy interactions (e.g., Veilleux, Kim, & Sanders 2002b). Large H I halos may also prevent dwarf galaxies from venting a wind (e.g., NGC 4449: Summers et al. 2003). Conversely, Strickland et al. (2004b) suggested that high-latitude hot gas above the disk can actually help the outflow to escape.

A popular way to estimate the escape fraction is to compare the outflow velocity with the local escape velocity derived from a gravitational model of the host galaxy. This is often a simple, truncated isothermal sphere. If truncated at $r_{\rm max}$, then the escape velocity $v_{\rm esc}$ at radius r is related to the rotation speed v_c and $r_{\rm max}$ by $v_{\rm esc}(r) = \sqrt{2}\ v_c\ [1 + ln(r_{\rm max}/r)]^{\frac{1}{2}}$. The escape velocity is not sensitive to the exact value of $r_{\rm max}/r$ [e.g., for $r_{\rm max}/r = 10 - 100$, $v_{\rm esc} \approx (2.6 - 3.3) \times v_c$]. The curve in Figure 6*a* is for $r_{\rm max}/r = 10$. If halo drag is tiny, material that exceeds $v_{\rm esc}$ may escape into the IGM. With this simple assumption, Rupke et al. (2005b) find that $\sim 5 - 10\%$ of the neutral material in starburst-driven winds will escape. This may only be a lower limit: much of the gas above $v_{\rm esc}$ may have already mixed with the IGM and would be invisible in Na I D absorption.

Given the correlation between outflow velocity and gas-phase temperature mentioned in §4.4, the escape fraction is surely larger for warm and hot phases. Indeed, warm gas in several dwarfs (including possibly M82) exceeds escape (e.g., Martin 1998; Devine & Bally 1999; Lehnert, Heckman, & Weaver 1999). Similarly, velocities derived in §4.4 from X-ray temperatures, $V_w \approx 500$ – 900 km s^{-1}, exceed escape for galaxies with $v_c \approx 130 - 300$ km s^{-1}. Recall that these are lower limits to the wind terminal velocities, so galaxies with $v_c \lesssim 130$ km s^{-1} may not retain hot, metal-enriched material (Martin 1999). As discussed in §7.1.2, this galaxy-mass dependence on metal retention makes definite predictions on the effective yield which appears to have been confirmed by observations.

4.7 Energy Injection Zone

HST images of nearby starbursts show that the star-forming regions can be extremely complex and luminous super-star clusters (SSCs), each having thousands of young ($\lesssim 50$ Myr) stars within a half-light radius $\lesssim 10$ pc. But the clustered part of star formation accounts for only $\sim 20\%$ of the integrated UV light in nearby optically-selected starbursts (Meurer et al. 1995). Most of the star formation is distributed diffusely in these objects. It is unclear which mode of star formation (clustered vs. diffuse) drives starburst winds. Both seem to in the outflow from the dwarf galaxy NGC 1569, whose wind seems to emanate from the entire stellar disk rather than just the central 100 pc near the SSCs (Martin et al. 2002). In M82, Shopbell & Bland-Hawthorn (1998) deduced from the diameter of the inner outflow cone a relatively large energy injection zone, ~ 400 pc. But chimneys at the base of the wind suggest localized venting of hot gas (Wills et al. 1999; see also Fig. 4). Heckman et al. (1990) used the gas pressure profile (Equation [10]) to deduce relatively large (a few hundred parsec) vertical sizes for the energy injection zones in several edge-on galaxies. But one should be wary of the possibility that the [S II] $\lambda\lambda$6716, 6731 emission lines that they used to derive density can be severely contamined by foreground or background disk emission; Veilleux et al. (1994) showed that this occurs in NGC 3079. Additionally, these may measure only vertical pressure profiles in the galaxy disk, not the pressure profile in the starburst.

Given the dependence of thermalization efficiency on density (§2.1.1), in high-

density environments diffuse star formation in the low-density ISM, not clustered star formation, may drive the wind most efficiently. Hence, Chevalier & Fransson (2001) have warned about using the radio continuum as a proxy for mechanical luminosity in starburst galaxies. Here, radio emission comes predominantly from SN remnants that are expanding in the dense ($\gtrsim 10^3 - 10^4$ H atoms cm^{-3}) interclump medium of molecular clouds. These radiate most of their mechanical energy, so they do not drive GWs. On the other hand, SNe that detonate in a lower-density medium heat gas and drive winds, but are largely invisible in the radio. The large gas densities at the centers of ULIRGs ($\sim 10^{4-5}$ cm^{-3}) (Downes & Solomon 1998; Bryant & Scoville 1999; Sakamoto et al. 1999) seem to imply a large volume filling factor of molecular clouds and possibly strong radiative losses, perhaps explaining the small mass entrainment efficiencies in ULIRGs (§4.5).

4.8 Excitation Properties & Evolution

Superbubbles and GWs are time-dependent, dynamic systems. How an outflow evolves is tied directly to the history of its energy source, *i.e.* the star formation history of the host (starburst versus quiescent star formation). As a GW evolves spatially (§§2.2 – 2.3), the gaseous excitation of any entrained material also changes because of two processes: (1) photoionization by hot OB stars in the starburst and by the hot X-ray-emitting wind, and (2) radiative shocks formed at the interface of the fast-moving wind and the slow-moving disk ISM. As expected from radiative shock models (Dopita & Sutherland 1995, 1996), the importance of shock-excited line emission relative to photoionization by the OB stars in the starburst appears to scale with the velocity of the outflowing gas (e.g., Lehnert & Heckman 1996; Veilleux et al. 2003; Rupke et al. 2005b). NGC 3079 is an extreme example of a shock-excited wind nebula, with outflow velocities > 1500 km s^{-1} (e.g., Filippenko & Sargent 1992; Veilleux et al. 1994). The excitation contrast between the star-forming host and the shock-excited wind material can in principle be exploited to search efficiently for GWs (Fig. 5*b*; Veilleux & Rupke 2002).

The dynamical state of an outflow also affects its gaseous excitation: Compact, pre-blowout superbubbles are less porous to ionizing radiation from hot stars than fragmented, post-blowout superbubbles or GWs. Such fine-tuning between outflow velocities and self-shielding of the starburst may explain why GWs dominated by OB-star photoionization are rare. "Inverted" ionization cones, where stellar photoionization dominates over shocks, have been detected in M82. This wind has cleared channels beyond the two prominent starbursting knots, allowing ionizing radiation to escape to large radii (Shopbell & Bland-Hawthorn 1998).

4.9 Wind Fluid

There is little direct evidence for the wind fluid in starbursts, because it is tenuous and hot, and therefore a poor X-ray radiator (e.g., Strickland & Stevens 2000; Strickland et al. 2000). The best evidence for it is in M82 (Griffiths et al. 2000;

Stevens et al. 2003), where the hottest gas is $\lesssim 75$ pc from the center, and has $T \sim 4 \times 10^7$ K and pressure $P/k \simeq 10^9$ K cm^{-3} if the X rays are mostly thermal (Griffiths et al. 2000). Then the hot fluid is overpressured relative to the disk ISM and drives the large-scale wind.

Hard (1 – 6 keV) X-ray emission is resolved in the dwarf galaxy NGC 1569 (Martin et al. 2002) and its temperature exceeds escape velocity (~ 80 – 110 km s^{-1}; Martin 1999). Interestingly, the spectral softening of X rays with radius that is expected from adiabatically cooling winds (e.g., Chevalier & Clegg 1985) is not seen, perhaps because of large mass loading.

The metal content of the X-ray-emitting gas may constrain mass loading, although significant theoretical and observational uncertainties remain. As discussed in §2.1.1, SN explosions are expected to dominate when GWs develop. So, the metallicity of the wind fluid is regulated by SNe yields. Unfortunately, the oxygen and iron yields of massive stars are only known to an accuracy of $\sim 2-3$ because of uncertainties in the critical $^{12}C(\alpha,\gamma)^{16}O$ reaction rate, and on the mass limit above which stars do not contribute to the yield (considerable reimplosion of heavy elements may affect stars of $\gtrsim 30$ M$_\odot$; e.g., Woosley & Weaver 1995). Determining the metallicity of X-ray-emitting gas observationally is notoriously difficult because of uncertainties in the atomic physics and because of the degeneracies inherent in fitting multi-component spectral models to data of low spectral resolution. The X-ray-emitting gas is a multi-phase medium with a range of temperatures, densities, and absolute/relative metal abundances, possibly located behind cool absorbing material of unknown metallicity and column density. The problem is therefore under-constrained and one must assume many unknowns. Presently there seems to be evidence that the α/Fe ratio is slightly super-solar in the inner wind of M82 (Stevens et al. 2003; Strickland et al. 2004a) and in the wind filaments of NGC 1569 (Martin et al. 2002), as expected if stellar ejecta from SNe II contribute to the wind fluid. If confirmed, these modest α/Fe enrichments would further support the idea that mass loading by disk material contributes significantly to the X-ray emission (recall the kinematic evidence for disk mass loading in §4.4). Martin et al. (2002) compared these measurements with predictions from SNe models of Woosley & Weaver (1995) to estimate a mass-loading factor of ~ 10 in NGC 1569.

4.10 Dust

Evidence is mounting that dust is often entrained in GWs (dust in the wind of our Galaxy was discussed in §3.2). Far-IR maps of a few GWs show extended cold dust emission along the galaxy minor axis, suggesting entrainment (e.g., Hughes, Robson, & Gear 1990; Hughes, Gear, & Robson 1994; Alton, Davies, & Bianchi 1999; Radovich, Kahanpää, & Lemke 2001). Color maps reveal elevated dust filaments in several GWs (e.g., NGC 1808: Phillips 1993; M82: Ichikawa et al. 1994; NGC 253: Sofue, Wakamatsu, & Malin 1994; NGC 3079: Cecil et al. 2001). In a few systems, including M82, extended polarized emission along the outflow axis indicates dust (e.g., Schmidt, Angel, & Cromwell 1976; Scarrott et

al. 1991, 1993; Alton et al. 1994; Draper et al. 1995). Extended red emission, a broad emission band commonly seen in galactic reflection nebulae, exists in the halo of M82 (Perrin, Darbon, & Sivan 1995; Gordon, Witt, & Friedmann 1998). Far-UV maps of M82 made with the *Ultraviolet Imaging Telescope* reveal a UV-bright southern cone that is consistent with scattering by dust in the wind (e.g., Marcum et al. 2001); recent *Galaxy Evolution Explorer* (GALEX) data confirm this conclusion (Hoopes et al. 2005). Other support for dusty outflows comes from the strong correlation between nuclear color excesses, $E(B-V)$, and the equivalent widths of blueshifted low-ionization lines in star-forming galaxies at low redshifts (e.g., Armus, Heckman, & Miley 1989; Veilleux et al. 1995b; Heckman et al. 2000).

Optical measurements can estimate dust masses if one knows the geometry of the dust filaments and the amount of foreground starlight and forward scattering. The dust mass in an outflow can best be estimated from far-IR data, despite uncertainties associated with the disk/halo decomposition and assumptions about the dust temperature distribution and emissivity law. Alton et al. (1999) estimate that ~ 2 – 10×10^6 $M_\odot$ of dust is outflowing from M82. Radovich et al. (2001) used the same technique to derive 0.5 – 3×10^6 $M_\odot$ of outflow into the halo of NGC 253. The dynamical times yield dust outflow rates of ~ 1 $M_\odot$ yr^{-1}.

The fate of this dust is uncertain; there are no direct constraints on its kinematics in outflows. However, the short sputtering timescale for silicate/graphite dust in GWs (e.g., Popescu et al. 2000; see also Aguirre 1999) suggests that grains of diameter $\lesssim 0.3\mu$m would not survive long if in direct contact with the wind. Moreover, there does not seem to be a tight spatial correlation between the extraplanar warm ionized medium of starbursts and quiescent galaxies and the dust filaments (e.g., Cecil et al. 2001; Rossa et al. 2004). Most likely, the dust is embedded in the neutral or molecular component of the outflow and shares its kinematics. Assuming a Galactic gas-to-dust ratio, the neutral gas outflow rates in LIRGs and ULIRGs (Rupke et al. 2005b) translate into dust outflow rates of ~ 0.1 – 10 $M_\odot$ yr^{-1}. Given the kinematics of the neutral gas and assuming no halo drag, $\sim 5-10\%$ of the entrained dust may escape the host galaxy. Wind-driven ejection of dust from galaxies may feed the reservoir of intergalactic dust (e.g., Stickel et al. 1998, 2002), although tidal interactions and ram-pressure stripping are also efficient conveyors of dust into the ICM of rich clusters.

5 LOCAL CENSUS OF LARGE-SCALE OUTFLOWS IN ACTIVE GALAXIES

The same methods detect outflows in nearby active galaxies and starburst-driven winds, so the same selection effects and observational limitations discussed in §4.1 apply. However, contrary to starburst-driven winds, winds associated with AGN need not be perpendicular to the galactic disk. Outflows directed close to the galactic disk are likely to be made very luminous by the high ambient densities. They are more easily observed in near face-on galaxies (e.g., M51: Cecil 1988; NGC 1068: Cecil, Bland, & Tully 1990). In a few systems, the orientation of an

inclined AGN disk can be determined independently from maser spots.

5.1 Detection Rate

As we discuss below, there is ample evidence for outflows in AGN from sub-kpc to galactic scale. But one must be aware of processes that may bias the interpretation of bipolar emission. Several active galaxies display kiloparsec-scale "ionization cones" that align with the radio axes of AGN rather than with the principle axes of the host galaxy (e.g., Wilson & Tsvetanov 1994; Kinney et al. 2000). They arise when ISM is illuminated by hard radiation from the AGN. Gas within the cones is more highly ionized than outside. Because the gas kinematics are unaffected by ionization, one should search for kinematic signatures to evaluate the frequency of occurrence of AGN outflows. Often, both outflows and ionization cones are present, e.g. NGC 1068 (Pogge 1988; Cecil et al. 1990), NGC 1365 (Veilleux et al. 2003), and NGC 4388 (Veilleux et al. 1999), emphasizing the need for high-quality kinematic data.

Circumnuclear starbursts in active galaxies are another complication. Half of all nearby, optically-selected Seyfert 2 galaxies also host a nuclear starburst (see, e.g., Cid Fernandes et al. 2001 and Veilleux 2001 and references therein); the fraction is larger in IR-selected systems. The sustaining conditions for nuclear activity (e.g., deep central potential with a reservoir of gas) also favor starburst activity and perhaps trigger starburst-driven GWs. This symbiotic relation between starbursts and AGN therefore complicates interpretation of GWs in AGN/starburst composites. For example, bipolar ionization cones can also arise in pure starburst galaxies (M82: Fig. 15 of Shopbell & Bland-Hawthorn 1998).

With these caveats, we revisit the detection of winds in active galaxies. Zensus (1997) reviewed the evidence for outflows in powerful radio-loud systems. Here we focus on Seyfert galaxies. Linear radio features suggestive of jet-like ejections on sub-kpc scales have long been known in 20 – 35% of Seyferts (e.g., Ulvestad & Wilson 1989; Morganti et al. 1999 and references therein); this is a lower limit because of limitations in spatial resolution ($\sim 1''$), sensitivity, and de-projection. New high-resolution images with the *Very Large Baseline Array* (VLBA) have indeed revealed jet-like outflows in previously unresolved sources and in low-luminosity AGN (Ho & Ulvestad 2001). As we describe below, optical studies of several Seyferts with linear radio structure show signs of jet-ISM interaction on a scale of tens of pc. Measurements of proper motion in a few bright sources confirm outwardly moving radio knots (e.g., Middelberg et al. 2004 and references therein). A jet interpretation is sometimes favored even when the radio emission is unresolved at the VLBI scale (e.g., Anderson, Ulvestad, & Ho 2004). Low-power, sub-kpc jets may exist in most Seyfert galaxies. Any thermal wind component cannot be established from the radio observations, yet there are speculations that it can be large (Bicknell et al. 1998).

Many active galaxies also show signs of large-scale, galactic outflows. In an optical study of a distance-limited sample of 22 edge-on Seyfert galaxies, Colbert et al. (1996a) found that $> 25\%$ have kinematic signatures of outflows or

extraplanar line emission out to $\gtrsim$ 1 kpc. The existence of extraplanar radio emission in 60% (6/10) supports this claim (Colbert et al. 1996b). Morphology and orientation suggest that this emission comes mainly from AGN-driven outflows (see §5.2). This detection rate is a lower limit because of sensitivity and selection effects. For instance, Baum et al. (1993) detected kiloparsec-scale extranuclear radio emission in $\sim$ 90% (12/13) of their objects, a sample of slightly more powerful, face-on Seyferts. The difference in detection rate may be due to small number statistics, differences in sample selection, or may indicate that some of this emission is associated with starburst-driven winds. Contamination by starburst-driven winds may also explain the large fraction ($11/12 \approx 90\%$) of starburst/Seyfert 2 composites with extended X-ray emission (Levenson, Weaver, & Heckman 2001a, 2001b). There is now irrefutable evidence that powerful AGN-driven outflows sometimes coexist with starburst-driven winds (e.g., NGC 3079: Cecil et al. 2001).

5.2 Morphology

Contrary to what we know of starburst-driven winds, AGN outflows are oriented randomly relative to the major axis of the host galaxy (e.g., Ulvestad & Wilson 1984; Kinney et al. 2000). Several well-known active galaxies, including NGC 1068 (Cecil et al. 1990), harbor a wide-angle outflow whose axis is not perpendicular to the galaxy disks and therefore interacts strongly with the disk ISM. Outflows near the disk plane are often well collimated (e.g., NGC 4258: Cecil et al 2000; ESO 428-G14: Falcke, Wilson, & Simpson 1998), until they collide with dense disk clouds or until they rise into the halo (e.g., NGC 4258: Wilson, Yang, & Cecil 2001). When the jet is drilling through the disk, detailed correspondence between radio and optical emission-line features indicates strong jet/ISM interactions over tens of pc (e.g., Falcke et al. 1998; Schmitt et al. 2003a, 2003b and references therein). The radio jets compress and shock ambient gas, enhancing line emission that may dominate the morphology of the NLR. The well-known correlation between radio and NLR luminosities supports a dynamical connection between the two (e.g., de Bruyn & Wilson 1978; Wilson & Willis 1980). A few jet deflections by ISM clouds are also seen (e.g., NGC 1068: Gallimore, Baum, & O'Dea 1996b; NGC 4258: Cecil et al. 2000; NGC 4151: Mundell et al. 2003). Jet/ISM interaction has also been mapped in X rays thanks to CXO (e.g., Young, Wilson, & Shopbell 2001; Wilson et al. 2001; Yang, Wilson, & Ferruit 2001).

In many edge-on systems, the radio structure has a linear or elongated morphology on subkiloparsec scale, but beyond the disk becomes more diffuse and wide-angled. The change may arise from the vertical pressure gradient in the surrounding ISM or from momentum loss within the sub-kpc NLR. The morphologies of the warm and hot ionized extraplanar gas are often correlated. They are distributed in a broad cone near the base of the outflow (e.g., NGC 2992: Colbert et al. 1998; Allen et al. 1999; Veilleux, Shopbell, & Miller 2001; Circinus: Veilleux & Bland-Hawthorn 1997; Smith & Wilson 2001) but become filamentary above the disk (e.g., NGC 4388: Veilleux et al. 1999, Fig. 5*c*; NGC 5506: Wilson,

Baldwin, & Ulvestad 1985). Spectacular bow shocks and finger-like structures are seen optically in the Circinus galaxy, perhaps due to the abnormally high gas content of this object (Fig. 5*d*; Veilleux & Bland-Hawthorn 1997). The correspondence between the extraplanar radio plasma and optical line-emitting material is often not as tight as that seen in the disk. Outflows with optical conical geometries may have very different radio morphologies: e.g., edge-brightened radio bubbles in NGC 2992 (Wehrle & Morris 1988) and Circinus (Elmouttie et al. 1998) but lumpy and filamentary radio structures in NGC 4388 and NGC 5506 (Colbert et al. 1996b). The extraplanar emission at radio wavelengths (where the foreground disk barely influences the emission) is sometimes lop-sided (e.g., NGC 4388) from asymmetric energy injection at the source or from asymmetric ISM on small scales.

5.3 Kinematics

Spatially resolved outflows are found on all scales in AGN. Relativistic outflows on parsec scales in powerful radio-loud sources are well established (Zensus 1997; Worrall & Birkinshaw 2004 and references therein). Recently, proper motions of radio components have been measured with VLBI in a few Seyfert galaxies (e.g., Middelberg et al. 2004 and references therein). These studies show that the outward motion of the radio components in these objects is non-relativistic ($\lesssim 0.25c$) on pc scales. There is now unambiguous kinematic evidence that these radio jets transfer momentum and energy to the ambient gas and drive some of the large-scale outflows seen in radio-quiet and radio-loud objects.

Gas in the NLR ($\sim$ 10 pc $-$ 1 kpc) and extended NLR (ENLR; $\gtrsim$ 1 kpc) is an excellent tracer of this jet/ISM interaction. The good match between nuclear emission-line widths and bulge gravitational velocities suggests that the gravitational component dominates in most Seyferts (Whittle 1985; Wilson & Heckman 1985; Veilleux 1991; Whittle 1992b; Nelson & Whittle 1996). But Seyferts with linear radio structures have long been known to have emission lines with complex profiles (e.g., Veilleux 1991) and supervirial velocity widths (e.g., Whittle 1992a) that implicate an additional source of KE in the NLR. Detailed long-slit spectra from the ground and from HST have presented evidence for a dynamical connection between the NLR and radio components in many of these galaxies (e.g., Whittle & Wilson 2004 and references therein). The complete spatio-kinematic coverage afforded by Fabry–Perot and integral-field spectrometers has constrained efficiently the intrinsic, 3D velocity fields of the outflowing ionized gas (e.g., Ferruit et al. 2004; Veilleux et al. 2002a and references therein). The signatures of jet-driven kinematics seen in some Seyfert galaxies are also detected in several powerful radio sources, particularly in compact steep-spectrum radio galaxies and quasars (e.g., Baum, Heckman, & van Breugel 1992; Gelderman & Whittle 1994; McCarthy, Baum, & Spinrad 1996; Best, Röttgering, & Longair 2000; Solórzano-Iñarrea, Tadhunter, & Axon 2001; O'Dea et al. 2002).

This large data set indicates that expanding radio lobes (Pedlar, Dyson, & Unger 1985) or bow shocks/cocoons driven by radio jets (Taylor, Dyson, & Axon

1992; Ferruit et al. 1997; Steffen et al. 1997a, 1997b) accelerate some of the line-emitting gas to ~ 100 – 1000 km s^{-1}. The fate of the gas clouds — whether undisturbed, destroyed, or accelerated — depends on factors such as the cloud mass, jet energy flux, and interaction geometry. Dense, molecular clouds in Seyfert galaxies can deflect radio jets by a significant angle without experiencing significant damage (e.g., NGC 1068: Gallimore et al. 1996a, 1996b; NGC 4258: Cecil et al. 2000). Jet-cloud interactions can be used to deduce key properties of the jet. In their analysis of the jet-molecular cloud interaction in the NLR of NGC 1068, Bicknell et al. (1998) argued that this jet (and perhaps those in other Seyferts) is heavily loaded with thermal gas and has low bulk velocities ($\sim 0.06c$), contrary to jets in powerful radio galaxies. Not surprisingly, the jets in Seyfert galaxies often deposit an important fraction of their KE well within ~ 1 kpc of the nucleus. The radial velocities of the emission-line knots in the NLRs of Seyfert galaxies show a slight tendency to increase out to ~ 100 pc from the nucleus then decrease beyond, whereas the line widths of the knots decrease monotonically with increasing distance from the nucleus (e.g., Crenshaw & Kraemer 2000; Ruiz et al. 2005). Deceleration beyond ~ 100 pc is likely due to drag from ambient gas.

Ram pressure from radio jets/lobes may not always dominate the acceleration of line-emitting gas in Seyfert galaxies. High-resolution studies with HST sometimes fail to find a one-to-one correspondence between the NLR cloud kinematics and the positions of the radio knots. Ram pressure from a diffuse, highly ionized wind or radiation pressure by the AGN radiation field has been suggested as the possible culprit in these cases (Kaiser et al. 2000; Ruiz et al. 2001). The high-velocity (~ 3000 km s^{-1}) line-emitting knots detected in NGC 1068 (Cecil et al. 2002b; Groves et al. 2004) may be explained by radiation pressure acting on dust grains in the clouds (Dopita et al. 2002). These knots may correspond to the well-known absorbers seen projected on the UV continua of some AGN (Crenshaw et al. 2003). Bright nuclear emission-line knots detected in several other nearby Seyfert galaxies may also contribute to the population of intrinsic UV absorbers (Crenshaw & Kraemer 2005; Ruiz et al. 2005).

Wind ram pressure or radiation pressure may also be responsible for blueshifted (~ 100 – 1000 km s^{-1}) neutral material detected in several AGN-dominated ULIRGs (Rupke, Veilleux, & Sanders 2005c), because few of them show jet-like radio structures. There is some evidence for higher average and maximum velocities in Seyfert-2 ULIRGs than in starburst-dominated ULIRGs, although the evidence for a strong influence of the AGN on these outflows is inconclusive. The situation is quite different among Seyfert-1 ULIRGs, where the outflows are driven mostly or solely by the AGN (Rupke, Veilleux, & Sanders 2005c; Fig. 6*a*). Similarly, nuclear activity is almost certainly responsible for the broad, blueshifted H I absorption wings detected in a growing number of compact radio galaxies. But here, jet-driven acceleration is implied (e.g., Morganti et al. 2003).

In Seyferts where the energy injection rate of the jet or wind suffices to eject radio/thermal plasma from the host galaxy, warm line-emitting gas is entrained into wide-angle outflows. The intrinsic, 3D velocity field of the line-emitting gas

over $\gtrsim 1$ kpc indicates roughly conical radial outflow with opening angles $2\theta \approx 60^\circ - 135^\circ$ and hollow (NGC 1365: Hjelm & Lindblad 1996; NGC 2992: Veilleux et al. 2001), partially filled (NGC 5506: Wilson et al. 1985), or filamentary geometry (Circinus: Veilleux & Bland-Hawthorn 1997; NGC 4388: Veilleux et al. 1999). Deprojected velocities are ~ 100 – 500 km s^{-1} in Seyferts, sometimes larger in radio galaxies. The geometry of the kinematic structures on large scales depends not only on the energy source but also on the galactic and intergalactic environment (e.g., the abnormally large gas content of Circinus may explain the peculiar filamentary morphology of its outflow). Rotation is sometimes detected in the velocity field of the outflowing gas (e.g., Circinus: Veilleux & Bland-Hawthorn 1997; NGC 2992: Veilleux et al. 2001), confirming that most of the line-emitting material comes from the disk ISM.

5.4 Mass Outflow Rates & Energetics

Kinematic deprojection is an essential prerequisite to meaningful dynamical analysis of AGN-driven winds. Data with complete spatio-kinematic coverage should be used to derive their masses and KE. We therefore discuss nearby ($z \lesssim 0.1$) objects for which spatially resolved kinematic data are available. The broad range of scales and velocities discussed in §§5.2 and 5.3 implies dynamical times for the entrained line-emitting material of $\sim 10^4$ – 10^6 years in the NLR (including the 3000 km s^{-1} knots in NGC 1068) and $\sim 10^6$ – 10^7 years in the ENLR.

Deriving ionized masses for AGN outflows follows the same steps as for starburst-driven winds, and therefore again favors high-density material (§4.5). Given uncertain volume filling factors, the warm ionized gas masses derived from optical data on Seyferts, $\sim 10^5$ – 10^7 M$_\odot$, are probably accurate to no better than about ± 0.5 dex. The corresponding mass outflow rates, $M/t_{\rm dyn} \approx 0.1 - 10\ M_\odot$ yr^{-1}, generally exceed tenfold the mass accretion rates necessary to fuel the AGN, indicating strong mass loading of the outflow by the galaxy ISM.

The KE of the warm ionized component in Seyfert galaxies is $\sim 10^{53}$ – 10^{56} erg, including both bulk and "turbulent" (spatially unresolved) motions. This range is similar to that in starburst-driven winds. Dynamical timescales yield KE outflow rates of $E_{\rm kin}/t_{\rm dyn} \approx 10^{40} - 10^{43}$ erg s^{-1}. The power radiated by Seyferts in line emission is 10 times larger and $\sim 10^2 - 10^4$ times larger than in the radio (e.g., Fig. 1 of Wilson, Ward, & Haniff 1988). Simple jet-driven models (Blandford & Königl 1979a, 1979b; Wilson 1981) reproduce these derived values using reasonable efficiency factors to relate jet and radio powers.

If the efficiency of energy/momentum transfer to the ambient material is nearly constant, both the entrained mass and KE scale with AGN luminosity (e.g., Baum & McCarthy 2000). Powerful quasars and radio galaxies with $L_{\rm bol} \sim 10^{45} - 10^{47}$ erg s^{-1} (not discussed so far) seem to have KE outflow rates that exceed those of Seyferts by several orders of magnitude. The KE of some outflows is comparable to the gravitational binding energy of gas in the host ($10^{58} - 10^{60}$ erg). Comparable energy is stored in the large radio lobes of radio-loud objects: $\gamma/(\gamma - 1)PV \sim 10^{58} - 10^{61}$ erg, where P and V are the pressure and volume

of the radio lobes, respectively, and $\gamma = 4/3$ is the mean adiabatic index of the relativistic fluid. Much of the energy dissipated by the AGN accretion disk appears to find its way into jet mechanical luminosity: powerful radio sources are Eddington-tuned engines with jet powers $Q \sim 0.1\ L_{\rm Edd}$ (Willott et al. 1999; see also Falcke, Malkan, & Biermann 1995).

Outflowing neutral gas detected in absorption in H I and Na I D in many AGN may add significant energy. Unfortunately, the mass of entrained neutral gas in these objects is poorly constrained because its location is unknown. The mass-conserving wind model of Rupke et al. (2005b; $R_{\rm outer} = 5$ kpc) applied to the Na I D absorption data on Seyfert 2 ULIRGs yields neutral mass outflow rates similar to those in starburst-driven winds, *i.e.* ~ 10 – $1000\ {\rm M}_\odot\ {\rm yr}^{-1}$. With this assumption, neutral-gas KEs and rates of $\sim 10^{56}$ – 10^{60} erg and $E_{\rm kin}/t_{\rm dyn} \approx 10^{41}-10^{45}$ erg s^{-1} are derived for Seyfert-2 ULIRGs, suggesting that this material may be a very important dynamical component of AGN-driven outflows.

5.5 Energy Injection Zone

An upper limit to the size of the energy injection zone of AGN-driven winds can be derived from the geometry of the optical outflow. Injection zones are often small enough to exclude a starburst origin for the wind. A good example is the Circinus galaxy (Fig. 5*d*), where the base of the outflow cone extends over $\lesssim 20$ pc, 10% of the size of the starburst (e.g., Smith & Wilson 2001 and references therein). The same technique has been used to measure the size of the primary energy source for the outflows in NGC 1068 ($\lesssim 50$ pc; e.g., Cecil et al. 1990; Arribas, Mediavilla, & Garcia-Lorenzo 1996; Garcia-Lorenzo, Mediavilla, & Arribas 1999), NGC 2992 ($\lesssim 100$ pc; Veilleux et al. 2001; Garcia-Lorenzo, Arribas, & Mediavilla 2001), and in several other jet-induced outflows (e.g., Whittle & Wilson 2004).

More accurate assessment of the energy source in AGN-driven winds often relies on detailed VLA, MERLIN, and VLBA radio maps of the central regions of AGN, down to scales below tens of parsecs. Radio emission generally resolves into a few compact sources, occasionally accompanied by elongated, jet-like features. On VLA scales, approximately half of all Seyfert galaxies contain at least one component with a flat or inverted radio spectrum (*i.e.* spectral slope $\alpha \geq -0.20$; e.g., Ulvestad & Ho 2001). Radio sizes are uncorrelated with Seyfert type, as expected from the unified scheme of AGN. On VLBI scales, $\gtrsim 80\%$ of sources are flat-spectrum (Middelberg et al. 2004; Anderson, Ulvestad, & Ho 2004), are often unresolved or only slightly resolved (~ 1 pc), and have brightness temperatures $> 10^7$ K. Synchrotron self-absorption from the base of the jet is the usual explanation for compact and flat- or inverted-spectrum radio emission from the central engines of radio galaxies. The same scenario is likely in some Seyfert galaxies and low-luminosity AGN. Free-free absorption by the nuclear torus or NLR may also occur. In NGC 1068, the flat-spectrum source has modest brightness temperature ($\sim 10^6$ K) and extends over ~ 1 pc perpendicular to the jet axis; this emission is believed to be optically thin, free-free emission from the ionized inner edge of the torus (Gallimore, Baum, & O'Dea 1997). Regardless of

the exact origin of the emission, the compact flat-spectrum component is thought to be the main energy source of the outflow, because of frequent alignment of the various radio components and from direct measurements of proper motions in a few objects (Middelberg et al. 2004 and references therein; see §5.3 above).

5.6 Source of Ionization

It is now generally agreed that the gas in Seyferts is photoionized by the nucleus, although whether spatial variations in line ratios result from a "classical" range of ionization parameters (e.g. Davidson & Netzer 1979), a range in the numbers of illuminated ionization- and matter-bounded clouds (Binette, Wilson, & Storchi-Bergmann 1996), or a dusty plasma at high ionization parameter (Dopita et al. 2002) are still discussed. The detection of X-ray cones coincident with the emission-line ionization cones in several Seyferts rules out photoionizing shocks as the primary source of ionization (e.g., Kinkhabwala et al. 2002; Iwasawa et al. 2003; Yang et al. 2001), although the relative importance of shocks almost certainly increases with jet power and the degree of interaction with the ambient medium (e.g., compact radio galaxies; Tadhunter 2002).

5.7 Dust

Dust is present in AGN outflows. Its reddening is evident in the narrow-line spectrum of radio-quiet and radio-loud galaxies (e.g., Osterbrock 1989 and references therein) and in the broad absorption line clouds of BAL QSOs (e.g., Crenshaw et al. 2003 and references therein). Dust has often been invoked to explain the extended blue wings in the narrow-line profiles (e.g, Veilleux 1991 and references therein), and in the IR continuum emission of several AGN (Barvainis 1987; Sanders et al. 1989; Pier & Krolik 1992). But more relevant to outflowing dust is that the correlation between color excess, $E(B-V)$, and the strength of the Na I D line noted for starburst galaxies is even stronger for AGN (Veilleux et al. 1995b). Dust outflow rates of ~ 0.1 – 10 $M_\odot$ yr^{-1} are inferred from the neutral-gas mass outflow rates discussed in §5.4, assuming the Galactic gas-to-dust ratio. These are comparable to the dust outflow rates in starburst galaxies (§4.10).

6 WINDS IN THE DISTANT UNIVERSE

6.1 High-Redshift Galaxies

There is evidence for winds in the spectra of several $z > 1$ galaxies. Low-ionization interstellar absorption lines that are blueshifted by hundreds of km s^{-1} relative to systemic velocities, and Lyα emission lines similarly shifted redward, have been detected in most $z \sim 3-4$ Lyman break galaxies (LBGs; e.g., Lowenthal et al. 1997; Pettini et al. 2000, 2001, 2002; Adelberger et al. 2003; Shapley et al. 2003), in several gravitationally lensed Lyα-emitting galaxies at $z \sim 4-5$ (e.g., Franx et al. 1997; Frye, Broadhurst, & Benitez 2002), and in many luminous IR galaxies at $z \gtrsim 2$ (e.g., Smail et al. 2003; Swinbank et al. 2005). Lyα emission with red

asymmetric or P Cygni-type profiles is also commonly seen in $z \gtrsim 5$ Lyα-emitting galaxies (e.g., Dey et al. 1998; Ellis et al. 2001; Dawson et al. 2002; Ajiki et al. 2002). A few isolated $z > 1$ line-emitting "blobs" and extended circumnuclear nebulae with complex structured velocity fields have been tentatively interpreted as spatially resolved large-scale winds driven by starbursts or AGNs (e.g., Francis et al. 2001; Ohyama, Taniguchi, & Shioya 2004 and references therein).

Prevalent winds in high-z galaxies, particularly in LBGs, are to be expected given their large surface densities of star formation: the typical size of the star-forming cores in LBGs is $r_{\rm half} \sim 1.6\ h_{70}^{-1}$ kpc (e.g., Giavalisco et al. 1996) and their SFRs are ~ 1 – 100 M$_\odot$ yr^{-1}. Thus, they have star formation surface densities $> 1\ M_\odot$ yr^{-1} kpc^{-2}. However, one should be cautious when applying local wind criteria to high-z galaxies because there are significant structural differences in starbursts between the two epochs. The energy injection zone in local starbursts is much smaller than the galaxy half-light radius and generally centered on the nucleus, whereas the starbursts in LBGs appear to be galaxy wide. The prominent disks of local starbursts were probably not yet assembled in $z \sim 3$ LBGs, perhaps resulting in more spherical winds than in local starbursts.

A well-studied wind in the gravitationally lensed LBG MS 1512−cB58 (Pettini et al. 1998, 2000, 2002) has bulk outflow velocity ~ 255 km s^{-1} on the basis of the positions of the low-ionization absorption lines relative to the rest-frame optical emission lines. Pettini et al. (2002) note that its outflow kinematics are remarkably symmetric: The profiles of the absorption lines from the different ionization stages are broadly similar, spanning a range of velocities of ~ 1000 km s^{-1}, whereas the receding portion of the outflow as mapped by the redshifted backscattered Lyα emission also has essentially the same kinematics. The derived mass outflow rate (~ 70 M$_\odot$ yr^{-1}) exceeds the SFR of this galaxy (SFR ≈ 40 M$_\odot$ yr^{-1}), so this outflow may have had a strong impact on the chemical evolution of the host galaxy. The entrained wind material appears to have enough energy to escape the gravitational potential of MS 1512−cB58 ($M_{\rm baryons} \sim 10^{10}$ M$_\odot$), but the large α/Fe ratio in the ISM of this object suggests that at least some of the material made by previous stellar generations is retained.

The properties of the outflow in MS 1512−cB58 seem to be typical of those in LBGs, although the data on fainter objects are necessarily more uncertain (Pettini et al. 2001; Adelberger et al. 2003; Shapley et al. 2003). Large velocity shifts averaging ~ 650 km s^{-1} are found by Shapley et al. (2003) between the low-ionization lines and the Lyα emission lines of LBGs. A comparison with the study of Pettini et al. (2001) suggests that these velocity offsets reduce to ~ 300 km s^{-1} when measured relative to the more reliable nebular lines. This value is slightly higher than the outflow velocities found in low-z galaxies of similar SFR's (§4.4).

The equivalent widths of blueshifted low-ionization interstellar absorption lines in LBGs anti-correlate strongly with the strength of the Lyα emission, and correlate with the color excess $E(B-V)$. The latter suggests that dust is entrained with the outflowing neutral gas and is sufficiently widespread to redden the host LBG; this effect is also observed in local wind galaxies (§4.10). The former is

easy to understand if we recall that the equivalent widths of saturated absorption lines (as is the case here) depend only on the covering fraction of the absorbing material and the range of velocities over which this material is absorbing. Larger covering factor or absorbing velocity interval implies that less Lyα emission can escape from the wind. This effect may also explain the redder UV continuum and the larger kinematic offsets between Lyα and the interstellar absorption lines observed in weak Lyα-emitting LBGs (Shapley et al. 2003).

Quantifying the environmental impact of LBG winds comes by probing the environment with spectra of background QSOs. Around six $z \sim 3$ LBGs, Adelberger et al. (2003) find hints of an H I deficit within comoving radius 0.5 h_{70}^{-1} Mpc. They favor a scenario whereby LBG winds influence the nearby IGM directly over a proximity effect caused by LBG-ionizing radiation. The excess of absorption-line systems with large C IV columns that they find near LBGs is interpreted as further evidence for chemical enrichment of the IGM by LBG winds, although it could also be attributed to debris from tidal interactions (e.g., Morris & van den Berg 1994).

In a recent extension to this survey, Adelberger et al. (2005) find that the relationship between C IV column density and clustering around LBGs is still present, although at a lower level than in the original survey. Most galaxies now appear to have significant H I within 1 h^{-1} Mpc of their centers, but some fraction of them ($\sim 1/3$) still show a significant deficit. The LBGs with strong H I absorption have roughly as much absorption as expected from windless, smoothed particle hydrodynamics (SPH) simulations of ΛCDM universes (e.g., Croft et al. 2002; Kollmeier et al. 2003), but LBGs without much H I are not present in these simulations. These results are at odds with the original suggestion of large, spherical windblown cavities around LBGs (Adelberger et al. 2003). They are qualitatively more consistent with the idea that winds emerge along paths of least resistance, possibly avoiding large-scale filaments (e.g., Theuns et al. 2002).

6.2 QSO Absorption-Line Systems

Large-scale GWs at all redshifts can be detected by their absorption of background QSO continuum light (e.g., Rauch 1998). Comparisons between the number densities of Mg II absorbers and star-forming galaxies and the properties of local outflows (e.g., Bond et al. 2001) suggest that there are enough Mg II absorbers to account for the expected properties of winds at $1 < z < 2$. But a more detailed analysis of absorption-line spectra is needed to answer this question quantitatively. Possible absorption signatures of winds or superbubbles include broad (few hundred km s^{-1}) and complex profiles pointing to strong nonrotational kinematics, a pairwise absorption pattern that straddles weak absorption near the kinematic center of the line, α-rich abundances, and large cloud-to-cloud variations in metallicity and ionization level. Such signals are evident in several very strong Mg II absorbers (Bond et al. 2001) and at lower column densities (e.g., Rauch et al. 2002; Zonak et al. 2004).

Detailed comparison of the kinematics of absorbers with those of the Mg II-

absorbing galaxies can further test for winds. In a study of five Mg II-absorbing galaxies at redshifts $0.44 < z < 0.66$ and of absorbers with projected impact parameters from those galaxies of $15 - 75\ h^{-1}$ kpc, Steidel et al. (2002) find that halo rotation sometimes dominates radial infall or outflow even for gas far from the galactic plane. But in the $z = 0.7450$ Mg II galaxy toward quasar Q1331+17, no absorbing gas is detected at the projected velocity of the disk rotation (Ellison, Mallén-Ornelas, & Sawicki 2003). The motion of the absorbing gas in this galaxy is consistent with a large ($\sim 30\ h_{70}^{-1}$ kpc) superbubble expanding at $\sim \pm 75$ km s^{-1}. Clearly, more data of high quality are needed for a final verdict (see, e.g., Côté et al. 2005).

7 THE SIGNIFICANCE OF GALACTIC WINDS

There is growing evidence that GWs have inhibited early star formation and have ejected a significant fraction of the baryons once found in galaxies. The latter may explain why few baryons are in stars ($\Omega_*/\Omega_b \sim 0.1$; Fukugita, Hogan, & Peebles 1998) and why galaxies like the Milky Way contain fewer than expected from hydrodynamical simulations (Silk 2003). We review in this section the impact of winds on galaxies and on their environment.

7.1 Influence of Winds on Galactic Scales

7.1.1 GALAXY LUMINOSITY FUNCTION GWs have modified substantially the shape of the galaxy luminosity function, flattening its faint-end slope compared to that of the halo mass function (e.g., Dekel & Silk 1986; Somerville & Primack 1999; Benson et al. 2003; Dekel & Woo 2003). The shallow potential of dwarf galaxies makes them vulnerable to photoevaporation (if $v_c \lesssim 10 - 15$ km s^{-1}; Barkana & Loeb 1999), mechanical feedback (e.g., de Young & Heckman 1994; MacLow & Ferrara 1999; Ferrara & Tolstoy 2000), and ablation by GWs from nearby galaxies (Scannapieco, Thacker, & Davis 2001). Significant feedback also appears necessary to avoid the 'cooling catastrophe' at high redshift that would otherwise overproduce massive luminous galaxies (e.g., Cole et al. 2000). Energies of a few $\times\ 10^{49}$ ergs per solar mass of stars formed can explain the sharp cutoff at the bright end of the luminosity function (Benson et al. 2003). Starburst-driven winds are too feeble by a factor of several to fully account for the cutoff. Benson et al. (2003) therefore argue that feedback from BH accretion is the only way to expel winds hot enough to prevent subsequent gas recapture by group halos. The kinetic power supplied by jets in radio-loud AGN, $Q \sim 0.1\ L_{\rm Edd}$ (see §5.4), may indeed suffice to account for the paucity of high-mass systems. Feedback from starburst- and AGN-driven winds may help set up the bi-modality observed in galaxy properties (see below; also Dekel & Birnboim 2005). AGN feedback may be particularly effective in clustered environment where the infalling gas is heated by a virial shock and thus more dilute.

7.1.2 CHEMICAL EVOLUTION In the GW scenario, massive galaxies with deep gravitational potentials are expected to retain more of their SN ejecta

than dwarf galaxies (e.g., Larson 1974; Wyse & Silk 1985; Dekel & Silk 1986; Vader 1986). Several authors have provided observational support for this picture, often using luminosity as a surrogate for mass (e.g., Bender, Burstein, & Faber 1993; Zaritsky et al. 1994; Jablonka, Martin, & Arimoto 1996; Trager et al. 1998; Kobulnicky & Zaritsky 1999; Salzer et al. 2005). An analysis of the Sloan Digital Sky Survey (SDSS) database by Tremonti et al. (2004) has shown that the gas-phase metallicity of local star-forming galaxies increases steeply with stellar mass from $10^{8.5}$ to $10^{10.5}$ $M_\odot h_{70}^{-2}$, but flattens above $10^{10.5}$ $M_\odot h_{70}^{-2}$. Similar trends are seen when internal velocity or surface brightness is considered instead of stellar mass (Kauffmann et al. 2003). The stellar mass scale of this flattening coincides roughly with the dynamical mass scale of metal retention derived by Garnett (2002). In that paper, Garnett used a simple closed-box chemical model to infer that the effective yield increases with galaxy mass up to the stellar yield obtained at $v_c \approx 125$ km s^{-1}. These results suggest that the chemical evolution of galaxies with $v_c \gtrsim 125$ km s^{-1} is unaffected by GWs, whereas galaxies below this threshold tend to lose a large fraction of their SN ejecta. This is consistent with estimates based on X-ray temperatures in wind galaxies (Sections 4.5, 4.6, and 4.9).

7.1.3 DISK SIZE AND DARK MATTER CONCENTRATION Hydrodynamical simulations reveal that dynamical friction from the inner dark halo acting on baryonic clumps overcompresses the galactic disk by a factor of five in radius compared what is observed (e.g., Steinmetz & Navarro 1999; Bullock et al. 2001). The suppression by stellar or AGN feedback of early gas cooling solves only part of this angular momentum problem (e.g., Sommer-Larsen, Götz, & Portinari 2003; Abadi et al. 2003). Entrainment and removal of material with low specific angular momentum by starburst- or AGN-driven GWs (e.g., Binney, Gerhard, & Silk 2001; Maller & Dekel 2002; Read & Gilmore 2005) is needed to explain the formation of exponential disks and the origin of bulge-less galaxies, especially if many bulges form by secular evolution (Kormendy & Kennicutt 2004). If many of the central baryons are thus ejected, CDM halo profiles become less cuspy (e.g., Navarro, Eke, & Frenk 1996) and more consistent with mass distributions observed in dwarfs and low-surface brightness galaxies (e.g., van den Bosch & Swaters 2001; de Blok, McGaugh, & Rubin 2001; Gentile et al. 2004; see Ricotti & Wilkinson 2004 for an alternative viewpoint).

It is interesting to speculate which of the structural properties observed in galaxies are due to the action of winds in the early universe. For example, it is well known that the average baryon density observed in a galaxy decreases with declining galaxy luminosity or mass (e.g. Kormendy 1985). As we have mentioned, it is probable that powerful central winds in the early galaxy can reshape the baryon density distribution in galaxies (e.g. van den Bosch 2001). This idea has been explored in many papers which incorporate centrally driven feedback processes in order to patch up the shortcomings of CDM simulations. Similarly, there is a decreasing baryon/dark matter fraction observed in galaxies with declining galaxy luminosity or mass (e.g. Persic, Salucci & Stel 1996; Mateo 1998). In a seminal paper, Dekel & Silk (1986) anticipated this now well-established

trend after considering the impact of SN-driven outflows in protodwarfs (see also Nulsen & Fabian 1997).

But there are reasons for believing that most of the feedback prescriptions imposed in CDM hydro simulations to date have little or no relevance to real galaxies (see Springel & Hernquist 2003 for a recent summary); many of the prescriptions manifestly do not conserve energy or entropy in the flow. When one considers the evolution of GWs in different environments, the trends (i.e. those arising from the action of winds) with total galaxy mass may be far less marked. For example, gas accretion onto a galaxy can staunch the developing outflow for any galaxy mass (e.g. Fujita et al. 2004; Springel & Hernquist 2003). Therefore, it is not obvious which of the structural properties can be ascribed to the action of winds at the present time.

7.1.4 POROSITY OF HOST ISM The relative contribution of AGN and starbursts to the inferred ionizing background depends critically on f_{esc}, the fraction of ionizing photons that escape from each object. The column densities of disks imply $\tau \approx 10^4 - 10^7$ at the Lyman edge, so leakage of ionizing radiation must be set by the topology of the ISM. GWs should play a key role in clearing a path for the escaping radiation (e.g., Dove, Shull, & Ferrara 2000), but this has not yet been confirmed observationally from constraints on f_{esc}. Hα measurements of high-velocity clouds above the disk of our Galaxy indicate that the escape fraction normal to the disk is 6% ($f_{esc} \approx 1\%$ – 2% averaged over 4π sr; Bland-Hawthorn & Maloney 1999, 2002). Estimates of the escape fraction in local, UV-bright starburst galaxies yield $f_{esc} \leq 6\%$ (Heckman et al. 2001b and references therein), and similar values are inferred for bright blue galaxies at $z = 1.1 - 1.4$ (Malkan, Webb, & Konopacky 2003). Star-forming galaxies thus contribute little ($< 15\%$) to the ionizing background at $z \lesssim 1.5$. The situation may be different at $z \gtrsim 3$, where the comoving number density of QSOs declines rapidly. Steidel, Pettini, & Adelberger (2001) infer $f_{esc} \approx 50 - 100\%$ for $\langle z \rangle = 3.4$ LBGs, but these results have been questioned by Giallongo et al. (2002), Fernández-Soto, Lanzetta, & Chen (2003), and Inoue et al. (2005). The dark cores of the saturated interstellar absorption lines in LBGs (Shapley et al. 2003) also appear inconsistent with large f_{esc}, unless we see little of the escaping ionizing radiation. The large value of f_{esc} inferred by Steidel et al. (2001), if confirmed, may be due to powerful GWs in these objects (§6.1).

7.1.5 SPHEROID – BLACK HOLE CONNECTION The masses of the central BHs in early-type galaxies and bulges correlate well with the velocity dispersions of the spheroidal component: $M_{\rm BH} = 1.5 \times 10^8 \sigma_{200}^4$ M$_\odot$ (Ferrarese & Merrit 2000; Gebhardt et al. 2000; Tremaine et al. 2002). This correlation is remarkably similar to the Faber–Jackson relation (Bernardi et al. 2003), and suggests a causal connection between galaxy formation and BH growth by means of a GW that regulates BH fueling (e.g., Silk & Rees 1998; Haehnelt et al. 1998; Fabian 1999; King 2003; Murray, Quataert, & Thompson 2005; Begelman & Nath 2005). The wind may be produced by the starburst that accompanied the formation of the spheroid or by the BH itself. An Eddington-like luminosity is

derived for the starburst or the BH, above which the growth of both spheroid and BH is stopped by the wind. In the case of a dominant BH wind, the Salpeter timescale, *i.e.* the timescale for $M_{\rm BH}$ to double, must be similar to the star formation timescale so that sufficient stars are formed before the BH wind blows away the ambient gas and stops star formation (Murray et al. 2005). The massive winds detected in nearby ULIRGs (§4.5) may be local examples of what might have occurred as spheroids formed (e.g., high-z LBGs and submm galaxies; §6.1).

7.2 Influence of Winds on Intergalactic Scales

7.2.1 INTRACLUSTER MEDIUM Galaxy clusters are excellent laboratories to study the impact of GWs on the environment because the hot, metal-enriched material ejected from SNe is retained by the cluster gravitational potential. Most metals in clusters are in the $\sim 0.3\ Z_\odot$ ICM, not in galaxies. Several lines of evidence suggest that GWs, not ram-pressure stripping, has dominated the transfer of metals from galaxies to ICM (see review by Renzini 2004). One is that ejection of hot gas from proto-galaxy GWs can create the 'entropy floor' (Kaiser 1991; Evrard & Henry 1991) necessary to explain the steep X-ray luminosity – temperature relation for nearby groups and clusters (e.g., Arnaud & Evrard 1999; Helsdon & Ponman 2000), the lack of cluster evolution out to $z \sim 1$ (e.g., Mushotzky & Scharf 1997), and the shallow density profiles of cooler groups (e.g., Horner et al. 1999). Heating of ~ 1 keV per gas particle would reproduce these results. Type II and Type Ia SNe (e.g., Lloyd-Davies, Ponman, & Cannon 2000), AGN (e.g., Cavaliere, Lapi, & Menci 2002), and Type II SNe from very massive, metal-poor progenitors (*i.e.* Population III stars; e.g., Loewenstein 2001) may all contribute to the heating.

Analyses of ICM abundances provide some constraints on the relative importance of these energy sources. Early reports of large α-element abundances in bright clusters by Mushotzky et al. (1996) first showed that Type II SNe enrich (and thus heat) some of the ICM. ASCA and XMM results now suggest that iron-rich Type Ia ejecta dominate in the centers of rich clusters, whereas the α-rich products of Type II SNe are distributed more evenly (e.g., Finoguenov et al. 2002, Tamura et al. 2004 and references therein). The iron mass scales with the optical light from the early-type galaxies and the cluster X-ray luminosity (e.g., Arnaud et al. 1992; de Grandi et al. 2004), suggesting iron enrichment by Type Ia SNe from these galaxies. A contribution from Population III stars may be needed to explain the inhomogeneity of α-elements in the ICM (Baumgartner et al. 2005). In-situ enrichment by intracluster stars may also be significant (Zaritsky, Gonzalez, & Zabludoff 2004).

AGN winds help enrich the ICM with metals, and the ubiquity of large "cavities" in the X-ray surface brightness of clusters with radio galaxies (e.g., Böhringer et al. 1993; Fabian et al. 2000; McNamara et al. 2000, 2001; Heinz et al. 2002; Mathews & Brighenti 2003) confirms that they modify the thermodynamics of the ICM. The hot, relativistic gas injected into the ICM by the AGN reduces, and perhaps even quenches, the mass accretion of cooling flows. The exact mecha-

nism by which energy in the radio bubbles turns into heat is still debated, but the absence of strong shocks along cavity walls, and the discovery of low-amplitude, semi-periodic ripples in the Perseus cluster (Fabian et al. 2003) suggest that viscous dissipation of sound waves may heat much of the inner ICM (see also Ruszkowski, Brüggen, & Begelman 2004a, 2004b; Reynolds et al. 2005). Other possible heaters include thermal conduction and turbulent mixing (e.g., Narayan & Medvedev 2001; Ruzkowski & Begelman 2002; Kim & Narayan 2003a, 2003b).

7.2.2 INTERGALACTIC MEDIUM The sphere of influence of GWs appears to extend to the low-density environment of the Lyα forest [N(H I) $\lesssim 10^{17}$ cm^{-2}]. Here, metallicities of 0.1% – 1% solar have been measured, with a possible excess of α-rich SN II products in the denser clouds (e.g., Rauch, Haehnelt, & Steinmetz 1997; Songaila 1997; Hellsten et al. 1997; Davé et al. 1998; Carswell, Shaye, & Kim 2002). The detection of metals in the IGM seems to favor momentum- over energy-driven winds (§2.3), or scenarios where the winds emerge along paths of least resistance without disturbing the filaments responsible for the Lyα forest (e.g., Theuns et al. 2002). Remarkably, both the column density distribution of C IV absorbers and its integral ($\Omega_{C\ IV}$) are invariant over $2 \lesssim z \lesssim 5$ (Songaila 2001; Pettini et al. 2003). One possible explanation is that most of the IGM metals are already in place by $z \sim 5$, perhaps from SN-driven outflows from low-mass subgalactic systems (e.g., Qian & Wasserburg 2005). Such systems may also be responsible for reionizing the IGM (Loeb & Barkana 2001 and references therein). However, this scenario does not completely explain why $\Omega_{\rm C\ IV}$ remains constant over this redshift range despite variations in the intensity and spectrum of the ionizing background (§7.1.4). Alternatively, the C IV systems are associated directly with GWs from LBGs at $z \lesssim 5$, and the constancy of $\Omega_{\rm C\ IV}$ arises instead from the flatness of the SFR density over $z \simeq 1.5 - 4$ (Adelberger et al. 2003). A critical discriminator between these two scenarios is to measure the metallicity in truly intergalactic clouds with N(H I) $\lesssim 10^{14}$ cm^{-2} (Cen, Nagamine, & Ostriker 2005). This is a portion of the Lyα forest that has not yet been explored in detail (although see Ellison et al. 2000).

8 FUTURE DIRECTIONS

Although great strides have been made over the past 25 years in understanding the physics and impact of GWs in the local and distant universe, much work remains to be done to quantify the role of these winds on the formation and evolution of galaxy-sized structures and the intergalactic environment. We now outline observational and theoretical issues that we feel deserve urgent attention.

8.1 Observational Challenges

8.1.1 UNBIASED CENSUS OF LOCAL WINDS As noted in §4.1, our current sample of GWs detects outflows that are sufficiently large and/or powerful but not so energetic as to expel all gas from their hosts. For example, the Galaxy's wind (§3.2) would be undetectable beyond the Local Group. While it

will be difficult to detect blown-away relics, there is a clear need to search the local volume systematically for winds. At optical wavelengths, the advent of tunable filters on 8-meter class telescopes will improve tenfold the sensitivity of optical wind surveys. These instruments will be ideal for searching for galaxies with starburst-driven winds through the contrast in gaseous excitation between wind and star-forming disk (§4.8). An IF spectrometer equipped with adaptive optics would complement tunable filters by providing densely sampled data on kinematics, filling factor, and excitation processes. CXO and XMM-Newton will continue to harvest high-quality data on the hot medium in GWs. New long-wavelength radio telescopes (e.g., GMRT, GBT, EVLA, and SKA) can better search for the relativistic component of GWs. Particularly important will be to determine the relative importance of GWs in dwarf and massive galaxies (§4.5).

8.1.2 WIND FLUID This component drives starburst-driven winds, yet has been detected in very few objects. Metal abundances suggest enrichment by SNe II, but the measurements are highly uncertain. Both sensitivity and high spatial resolution are needed to isolate the hot wind fluid from X-ray stellar binaries and the rest of the X-ray-emitting gas. But, no such instrument is planned for the foreseeable future. Indirect methods that rely on the properties of gas in the energy injection zone to constrain the wind pressure may be necessary. Current measurements of the pressure profiles in wind galaxies are certainly contaminated by the foreground/background disk ISM. Measurements in the mid- or far-IR with the *Spitzer Space Telescope* (SST) and *Herschel Space Observatory* will reduce the effects of dust obscuration.

8.1.3 ENTRAINED MOLECULAR GAS & DUST Despite the important role of the molecular component in GWs, high-quality mm-wave data exist only for M82. This is due to the limited sensitivity and spatial resolution of current instruments, but this will change soon. New mm-wave arrays (e.g., CARMA, and especially ALMA) will map the molecular gas in a large sample of nearby galaxies with excellent resolution ($< 1''$). Sub-mm and mid-IR data from the ground (e.g., SMA, JCMT, CSO) and from space (e.g., SST and Herschel) will constrain the amount and location of dust in the winds.

8.1.4 ZONE OF INFLUENCE & ESCAPE EFFICIENCY The environmental impact of GWs depends on the size of their zone of influence and on the fraction of wind fluid and entrained ISM that can vent from their hosts. Very deep emission-line, X-ray, and radio data on large scale would help tremendously to constrain wind extent. Tunable filters on 8-meter class telescopes may be particularly useful here. Absorption-line studies of bright background galaxies (e.g., high-z quasars, LBGs) have proven to be a very powerful tool to constrain the zone of influence of GWs at large redshifts. The Cosmic Origins Spectrograph (COS) on HST could extend the sample to a larger set of wind galaxies. Deep 21-cm maps of GW hosts on scales of up to $\sim$ 100 kpc would help to quantify the effects of halo drag. The escape efficiency of winds may also be constrained indirectly by measuring the stellar metallicities of galaxies suspected to have experienced GWs (e.g., largely gas-free dwarf spheroids in the Local Group) and

then comparing these values with the predictions of leaky-box models (e.g., Lanfrancini & Matteucci 2004).

8.1.5 THERMALIZATION EFFICIENCY Observational constraints on the thermalization efficiency of GWs are rare because of an incomplete accounting of the various sources of thermal energy and KE in the wind. A multiwavelength approach that considers all gas phases is needed.

8.1.6 WIND/ISM INTERFACE & MAGNETIC FIELDS Constraints on microphysics at the interface between the wind and galaxy ISM are available in only a handful of galaxies. High-resolution ($\lesssim$ parsec scale) imaging and spectra of the entrained disk material in a sizable sample of local objects are required. The large-scale morphology of the magnetic field lines has been mapped in a few winds, but the strength of the field on pc scale is unknown. This information is crucial in estimating the conductivity between the hot and cold fluids.

8.1.7 GALACTIC WINDS IN THE DISTANT UNIVERSE Absorption-line studies of high-z galaxies and QSOs will remain a powerful tool to search for distant GWs and to constrain their environmental impact. Future large ground and space telescopes will extend such studies to the reionization epoch. These galaxies are very faint, but gravitational lensing by foreground clusters can make them detectable and even spatially resolved. Cross-correlation analyses of wind galaxy surveys with detailed maps of the cosmic background radiation (CBR) (e.g., from the Planck mission) may also help to constrain the extent of the hot medium in winds by means of the Sunyaev-Zel'dovich effect (e.g., Voit 1994; Scannapieco & Broadhurst 2001), although one will need to consider all other foreground sources that affect the CBR (Hernàndez-Monteagudo, Genova-Santos, & Atrio-Barandela 2004 and references therein).

8.1.8 POSITIVE FEEDBACK BY WINDS Star-forming radio jet/gas interactions have been found in a few nearby systems (e.g., Minkowski's Object: van Breugel et al. 1985; Cen A: Oosterloo & Morganti 2005) and are suspected to be responsible for the "alignment effect" between the radio and UV continua in distant radio galaxies (e.g., van Breugel et al. 2004 and references therein). The same physics may also provide positive feedback in wind galaxies. Convincing evidence for superbubble-induced star formation has recently been found in the disk of our own Galaxy (Oey et al. 2005). In §4.3 we noted that shocked H_2 gas and circumnuclear rings of H II regions in a few wind galaxies may represent wind-induced star formation at the contact discontinuity/ISM shock associated with lateral stagnation of the wind in the galaxy disk. This region is also a gas reservoir from which to fuel the starburst. We do not know how often such rings form. Excess free-free emission on the inner edge of the outflow near the disk in M82 has been interpreted as a wind-induced starburst (Matsushita et al. 2004). A galaxy companion within the zone of influence of a GW may also be searched for wind-induced starburst activity (e.g., Irwin et al. 1987). This effect may have triggered the starburst in NGC 3073, a companion to NGC 3079 (e.g., Filippenko & Sargent 1992).

8.2 Theoretical Challenges

8.2.1 MODELING THE ENERGY SOURCE Current simulations do a poor job of modeling the energy source itself, especially in AGN-driven winds where energy and momentum injection rates are virtually unknown. Deeper understanding of AGN jets and winds is needed before simulating the impact of AGN-driven outflows. The situation for starburst-driven winds is much better, but the input energetics are still highly uncertain because the thermalization efficiency is constrained poorly by observation and theory. Simulations by Thornton et al. (1998) have shown that radiative losses of SN remnants expanding into *uniform* media of $\sim 0.02 - 10$ cm^{-3} are $\sim 0\% - 90\%$. But, it would be useful to run more realistic simulations with a range of molecular filling factors for young star clusters that evolve within a multiphase ISM.

8.2.2 MODELING THE HOST ISM The work of Sutherland et al. (2003b) noted in §2.4 is the first of a new generation of simulations able to handle a multiphase ISM with a broad range of densities and temperatures. Such sophistication is crucial to understanding and predicting the mass of gas entrained in winds. As discussed in §2.4, simulations show that the initial encounter of clouds with a wind drives a strong shock that may devastate the clouds. Once in ram-pressure equilibrium with the wind, however, clouds may accelerate to a significant fraction of the wind velocity before RT and KH instabilities shred them. To test the survival of entrained gas, these hydro processes should be combined with the effects of conductive evaporation to model the interface between the hot wind fluid and the dense ISM clouds. On the large scale, it will be important to use realistic distributions for the galaxy ISM, accounting for the clumpiness of the halo component and the disk (e.g., Fig. 1), and possible large-scale magnetic fields. These simulations would quantify the drag of the halo gas, the impact of wind on disk ISM, and the feedback from wind-induced star formation.

8.2.3 COUPLING THE RADIATION FIELD TO GAS Current simulations do not account for possible coupling between the wind material and the radiation field emitted by the energy source or the wind itself, and indeed ignore radiation pressure. For instance, thick, dusty ISM clouds entrained in the wind may be photoionized by the hot wind fluid and radiative shocks at the wind/ISM interface, with major impact on their gaseous ionization.

Acknowledgements This article was begun while S.V. was on sabbatical at the California Institute of Technology and the Observatories of the Carnegie Institution of Washington; this author thanks both institutions for their hospitality. G.C. thanks CTIO for its hospitality. We thank the scientific editor, J. Kormendy, for constructive comments on the style and contents of this review, and S. Aalto, P.-A. Duc, R. Braun, D. Forbes, L. Tacconi, D. Calzetti for organizing recent conferences that provided excellent venues to discuss many of the issues reviewed here. S.V. acknowledges partial support of this research by NSF/CAREER grant AST-9874973.

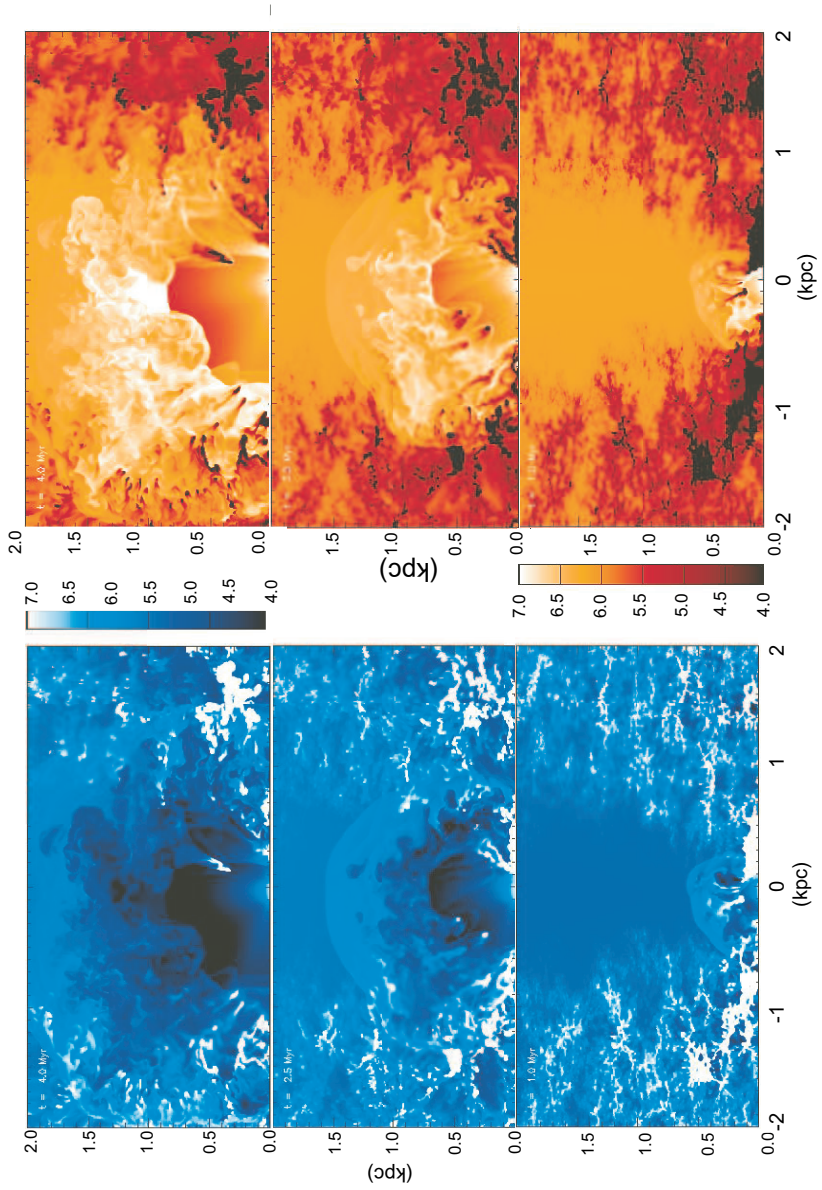

Figure 1: An example of a state-of-the-art 3D hydrodynamical simulation of a starburst outflow in an ISM with fractal size distribution at three epochs after the constant energy input wind starts to blow: 1.0 Myr (bottom), 2.5 Myr (middle), and 4.0 Myr (top). Blue is log-density and red is log-temperature (courtesy J. Cooper, G. Bicknell, R. Sutherland).

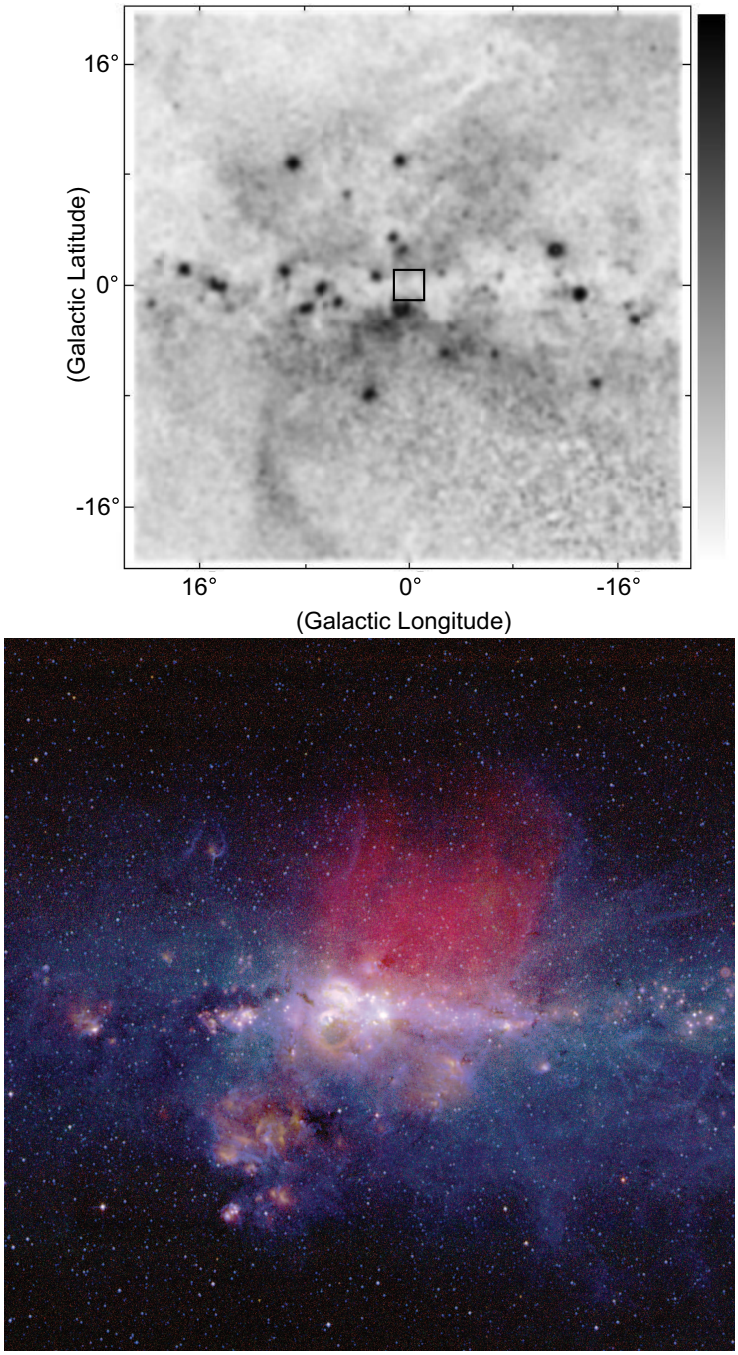

Figure 2: Aspects of the Milky Way's wind. (top) ROSAT 1.5 keV diffuse X-ray map that shows a biconical pattern emerging from the Galactic Center on scales of tens of degrees. (bottom) The inner $\sim 2.5 \times 2.5^\circ$ around the Galactic Center. Above the plane in red is the Galactic Center Lobe (GCL), here imaged by Law & Yusef-Zadeh with rasters from the Green Bank Telescope (GBT). Elsewhere, the color image comes from 8.3 (B), ~ 13 (G), and 21.3 (R) μm scans obtained with the SPIRIT III radiometer on the MSX spacecraft. These show embedded dust at various temperatures. Note the warm dust filaments along the edges of the GCL.

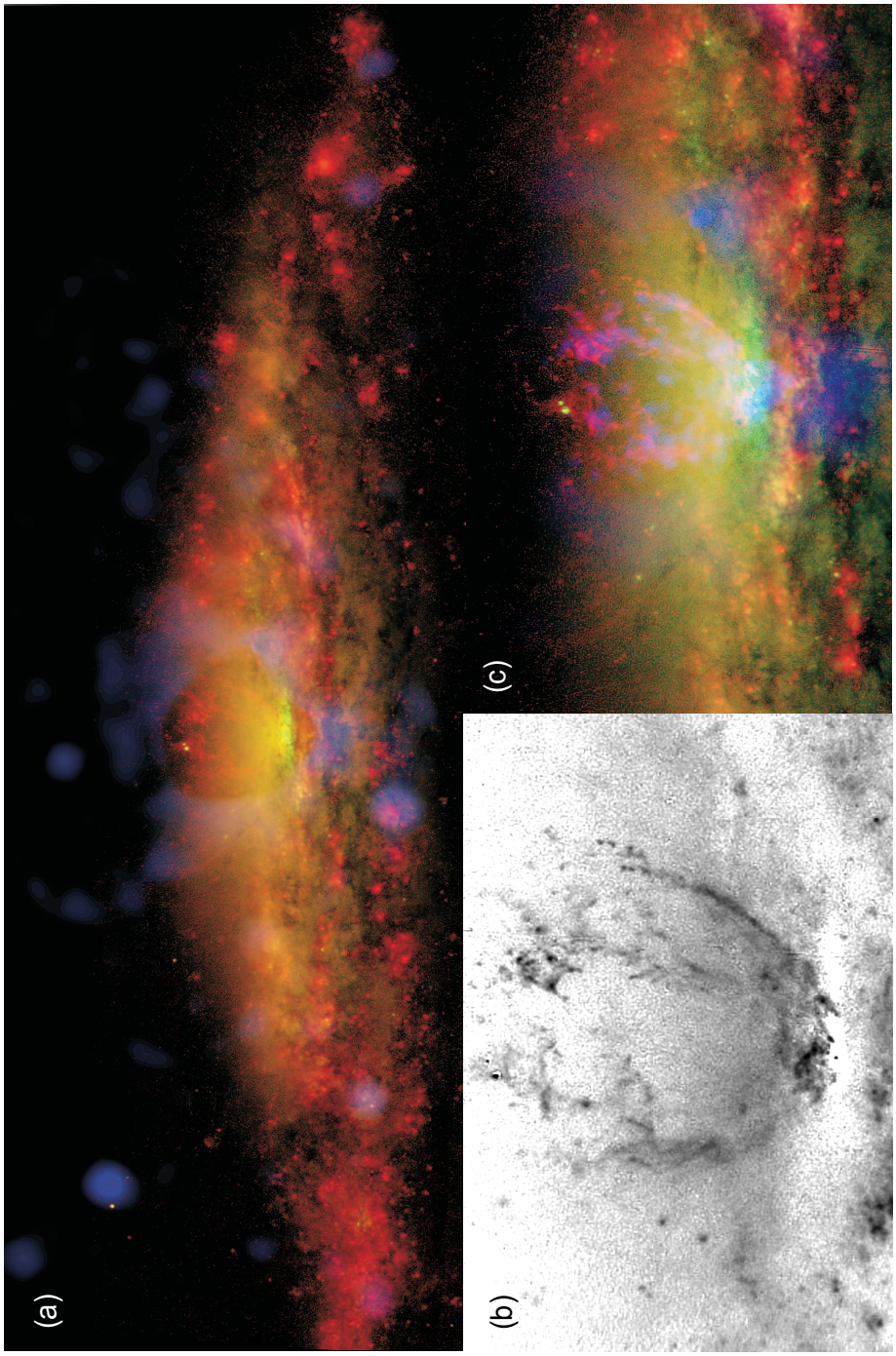

Figure 3: NGC 3079 imaged with HST (red for Hα+[N II], green for I-band) and CXO (blue). (a) large-scale emission across 15×5 kpc. Numerous Hα filaments rise above the disk. Note the V-shaped wind pattern extending in X rays from nucleus; for clarity, we have suppressed the diffuse X-ray emission across the superbubble, where it is generally clumped (see [c]). (b) The 1×1.2 kpc superbubble in Hα+[N II] emission, with log-scaled intensities. It is composed of 4 vertical towers of twisted filaments; the towers have strikingly similar morphologies. (c) Close-up of the wind-swept, circumnuclear region. Note how X-ray emission (blue) clumps along the optical filaments of the superbubble at the limit of CXO's resolution. A prominent dust filament at left drops out of the wind.

Figure 4: M82, imaged by the WIYN telescope in Hα (magenta) and HST in BVI continuum colors (courtesy Smith, Gallagher, & Westmoquette). Several of the largest scale filaments trace all the way back to super-starclusters embedded in the disk.

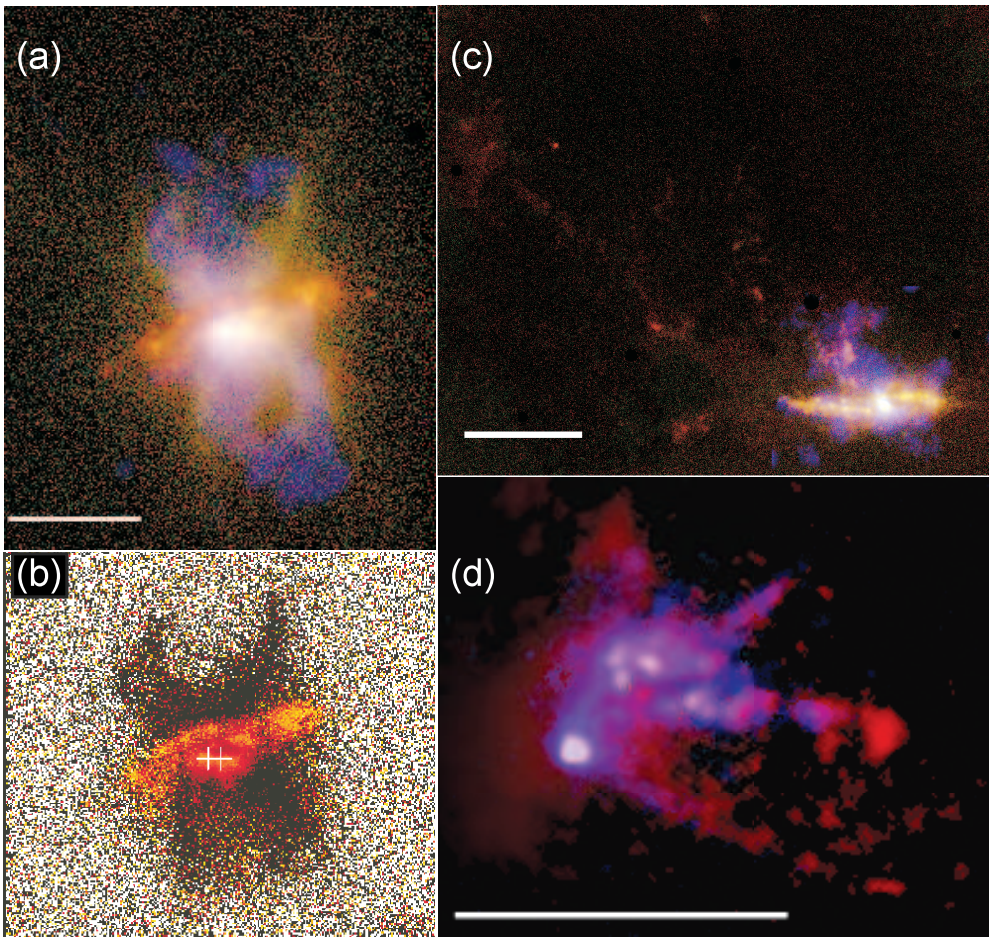

Figure 5: (a) Starburst galaxy NGC 1482 imaged in Hα (red), [N II] (green), and CXO (blue). The bar is 3 kpc long. For this and the other three panels, N is up and E is left, and intensities in all bands are log-scaled. (b) Excitation map of NGC 1482 showing the shock-excited ([N II] λ6583/Hα $\gtrsim$ 1 in black), biconical structure due to the wind above and below the star-forming disk ([N II]/Hα $<$ 1 in orange). The scale is the same as in (a), and the white crosses indicate the locations of two bright star-forming regions in the disk. (c) Seyfert galaxy NGC 4388 imaged in Hα (red), [N II] (green), and CXO (blue). The bar is 8 kpc long. The kinematics of the extraplanar gas $\lesssim$ 8 kpc north of the nucleus are dominated by the AGN-driven outflow. The long Hα trail extending further to the north-east may be due to ram-pressure stripping by the ICM in the Virgo cluster. (d) Central region of the Circinus galaxy imaged in [O III] (blue) and blueshifted (between –150 and 0 km s^{-1}) Hα (red). The bar is 1 kpc long. The [O III] emission traces the ionization cone and conical wind produced by the AGN, whereas the Hα emission immediately north and east of the nucleus is dominated by the circumnuclear starburst. Spectacular filaments and bow shocks are seen on scales of $\sim$ 500 – 900 pc.

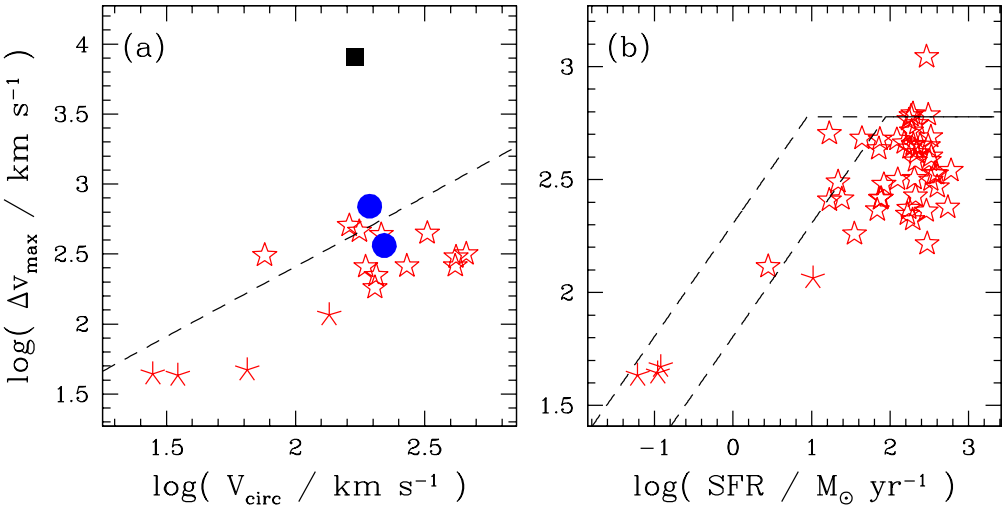

Figure 6: Maximum Na I D absorption-line outflow velocities as a function of (a) circular velocities, and (b) star formation rates. Red skeletal stars are star-forming dwarfs from Schwartz & Martin (2004) and red open stars are infrared-selected starbursts from Rupke et al. (2005a, 2005b). Filled blue circles and filled black squares are Seyfert 2s and Seyfert 1s from Rupke et al. (2005c). The dashed line in (a) represents the escape velocity for a singular isothermal sphere with $r_{max}/r = 10$, whereas the dashed lines in (b) are characteristic velocities of ram-pressure accelerated clouds (Murray et al. 2005) for column densities of 10^{20} cm^{-2} (top line) and 10^{21} cm^{-2}.

Literature Cited

Abadi MG, Navarro JF, Steinmetz M, Eke VR. 2003. ApJ 591:499

Adelberger KL, Shapley AE, Steidel CC, Pettini M, Erb DK, Reddy NA. 2005. ApJ In press

Adelberger KL, Steidel CC, Shapley AE, Pettini M. 2003. ApJ 584:45

Agol E, Krolik J. 1999. ApJ 524:49

Aguirre A. 1999. ApJ 525:583

Ajiki M, Taniguchi Y, Murayama T, Nagao T, Veilleux S, et al. 2002. ApJ 576:L25

Allen MG, Dopita MA, Tsvetanov ZI, Sutherland RS. 1999. ApJ 511:686

Allen RJ, Sancisi R, Baldwin JE. 1978:A&A 62:397

Alton PB, Davies JI, Bianchi S. 1999. A&A 343:51

Alton PB, Draper PW, Gledhill TM, Stockdale DP, Scarrot SM, Wolstencroft RD. 1994. MNRAS 270:238

Anderson JM, Ulvestad JS, Ho LC. 2004. ApJ 603:42

Armus L, Heckman T, Miley G. 1989. ApJ 347:727

Arnaud M, Evrard AE. 1999. MNRAS 305:631

Arnaud M, Rothenflug R, Boulade O, Vigroux L, Vangioni-Flam E. 1992. A&A 254:49

Arribas S, Mediavilla E, Garcia-Lorenzo B. 1996. ApJ 463:509

Baganoff FK, Maeda Y, Morris M, Bautz MW, Brandt WN, et al. 2003. ApJ 591:891

Baldwin JE. 1955. MNRAS 115:684

Bally J, Stark AA, Wilson RW, Henkel C. 1988. ApJ 324:223

Balsara DS, Krolik JH. 1993. ApJ 402:109

Barkana R, Loeb A. 1999. ApJ 523:54

Barvainis R. 1987. ApJ 320:537

Baum SA, Heckman TM, van Breugel WJM. 1992. ApJ 389:208

Baum SA, McCarthy PJ. 2000. AJ 119:2634

Baum SA, O'Dea CP, Dallacassa D, de Bruyn AG, Pedlar A 1993. ApJ 419:553

Baumgartner W, Loewenstein M, Horner DJ, Mushotzky RF. 2005. ApJ 620:680

Begelman MC. 1985. ApJ 297:492

Begelman MC, McKee CF Shields GA. 1983. ApJ 271:70

Begelman MC, Nath BM. 2005. MNRAS in press astro-ph/0504400

Bender R, Burstein D, Faber SM. 1993. ApJ 411:153

Benson AJ, Bower RG, Frenk CS, Lacey CF, Baugh CM, Cole S. 2003. ApJ 599:38

Berkhuijsen E. 1972. AA Suppl, 5:263

Bernardi M, Sheth RK, Annis J, Burles S, Eisenstein DJ, et al. 2003. AJ 125:1849

Best PN, Röttgering HJA, Longair MS. 2000. MNRAS 311:23

Bicknell GV, Dopita MA, Tsvetanov ZI, Sutherland RS. 1998. ApJ 495:680

Binette L, Wilson AS, Storchi-Bergmann T. 1996. A&A 312:365

Binney J, Gerhard O, Silk J 2001. MNRAS 321:471

Bland J, Tully RB. 1988. Nature 334:43

Blandford RD, Königl A. 1979b. ApJ 232:34

Blandford RD, Königl A. 1979a. AstrophysLett, 20:15

Blandford RD, Payne DG. 1982. MNRAS 199:883

Bland-Hawthorn J, Cohen M. 2003. ApJ 582:246

Bland-Hawthorn J, Maloney PR. 1999. ApJ 510:L33

Bland-Hawthorn J, Maloney PR. 2002. ASP Conf. Extragalactic Gas at Low Redshift, held at the Carnegie Observatories, Pasadena, California, Vol. #254, ed. J Mulchaey, J Stocke, 267. San Francisco: ASP

Böhringer H, Voges W, Fabian A, C, Edge AC, Neumann DM. 1993. MNRAS 264:L25

Bond NA, Churchill CW, Charlton JC, Vogt SS. 2001. ApJ 562:641

Brandl B. 2005. in Starbursts: From 30 Doradus to Lyman Break Galaxies, eds R de Grijs and RM Gonzalez Delgado in press astro-ph/0501572

Brandl B, Sams BJ, Bertoldi F, Eckart A, Genzel R, et al. 1996. ApJ 466:254

Braun R. 1985. PhD thesis University of Leiden Netherlands, 182 pp.

Breitschwerdt D, Schmutzler T. 1999. A&A 347:650

Bryant PM, Scoville NZ. 1999. AJ 117:2632

Bullock J. S, Dekel A, Kolatt TS, Kravtsov AV, Klypin AA, Porciani C, Primack JR. 2001. ApJ 555:240

Burbidge E, M, Burbidge GR, Rubin VC. 1964. ApJ 140:942

Burbidge GR, Hoyle F. 1963. ApJ 138:57
Burke JA. 1968. MNRAS 140:241
Cannon JM, Skillman ED, Sembach KR, Bomans DJ. 2005. ApJ 618:247
Cantó J, Raga AC, Rodriguez LF. 2000. ApJ 536:896
Carilli CL, Holdaway MA, Ho PTP, de Pree CG. 1992. ApJ 399:L59
Carswell RF, Shaye J, Kim T.-S. 2002. ApJ 578:43
Castor J, McCray R, Weaver R. 1975. ApJ 200:L107
Cavaliere A, Lapi A, Menci N 2002. ApJ 581:L1
Cecil G. 1988. ApJ 329:38
Cecil G, Bland J, Tully RB. 1990. ApJ 355:70
Cecil G, Bland-Hawthorn J, Veilleux S. 2002a. ApJ 576:745
Cecil G, Bland-Hawthorn J, Veilleux S, Filippenko AV. 2001. ApJ 555:338
Cecil G, Dopita MA, Groves B, Wilson AS, Ferruit P, Pcontal E, Binette L. 2002b. ApJ 568:627
Cecil G, Greenhill LJ, DePree CG, Nagar N, Wilson AS, Dopita MA, Pérez-Fournon I, et al. 2000. ApJ 536:675
Cen R, Nagamine K, Ostriker JP. 2005. ApJ in press astro-ph/0407143
Cheng LX, Leventhal M, Smith DM, Purcell WR, Tueller J, et al. 1997. ApJ 481:L43
Chevalier RA. 1992. ApJ 397:L39
Chevalier RA, Clegg AW. 1985. Nature 317:44
Chevalier RA, Franson C. 2001. ApJ 558:L27
Chu Y.-H, Kennicutt RC, Jr. 1994. ApJ 425:720
Cid Fernandes R, Heckman T, Schmitt H, González Delgado RM, Storchi-Bergmann T. 2001. ApJ 558:81
Colbert EJM, Baum SA, Gallimore JF, O'Dea CP, Chistensen JA. 1996b. ApJ 467:551
Colbert EJM, Baum SA, Gallimore JF, O'Dea CP, Lehnert MD, et al. 1996a. ApJS 105:75
Colbert EJM, Baum SA, O'Dea CP, Veilleux S. 1998. ApJ 496:786
Cole S, Lacey CG, Baugh CM, Frenk CS. 2000. MNRAS 319:168
Côté S, Wyse RFG, Carignan C, Freeman KC, Broadhurst T. 2005. ApJ 618:178
Cowie LL, McKee CF, Ostriker JP. 1981. ApJ 247:908
Crenshaw DM, Kraemer SB. 2000. ApJ 532:L101
Crenshaw DM, Kraemer SB. 2005. ApJ in press astro-ph/0501257
Crenshaw DM, Kraemer SB, George IM 2003. ARA&A 41:117
Croft RAC, Hernquist L, Springel V, Westover M, White M. 2002. ApJ 580:634
Dahlem M, Lazendic JS, Haynes RF, Ehle M, Lisenfeld U. 2001. A&A 374:42
Dahlem M, Weaver KA, Heckman TM. 1998. ApJS 118:401
Davé R, Hellsten U, Hernquist L, Katz N, Weinberg DV. 1998. ApJ 509:661 Davidson K, Netzer H. 1979. RevModPhys 51:715
Dawson S, Spinrad H, Stern D, Dey A, van Breugel W, de Vries W, Reuland M. 2002. ApJ 570:92
de Grandi S, Ettori S, Longhetti M, Molendi S. 2004. A&A 419:7
Dekel A, Birnboim Y. 2005. ApJ in press astro-ph/0412300
Dekel A, Silk J. 1986. ApJ 303:39
Dekel A, Woo J. 2003. MNRAS 344:1131
de Blok WJG, McGaugh SS, Rubin VC. 2001. AJ 122:2396
de Bruyn AG, Wilson AS. 1978:A&A 64:433
de Young DS, Heckman TM. 1994. ApJ 431:598
D'Ercole A, Brighenti F, 1999. MNRAS 309:941
Dey A, Spinrad H, Stern D, Graham JR, Chaffee FH. 1998. ApJ 498:L93
Dettmar RJ. 1992. Fundamentals of Cosmic Physics 15:143
Devine D, Bally J. 1999. ApJ 510:197
Dopita MA, Groves BA, Sutherland RS, Binette L, Cecil G. 2002. ApJ 572:753
Dopita MA, Sutherland RS. 1995. ApJ 455:468
Dopita MA, Sutherland RS. 1996. ApJS 102:161
Dove J, Shull JM, Ferrara A. 2000. ApJ 531:846
Downes D, Solomon PM. 1998. ApJ 507:615
Draper PW, Done C, Scarrot SM, Stockdale DP. 1995. MNRAS 277:1430
Duric N, Seaquist ER. 1988. ApJ 326:574
Eckart A, Ott T, Genzel R. 1999. A&A 352:L22

Efstathiou G. 2000. MNRAS 317:697
Ehle M. 2005. in Extra-planar Gas, ed R Braun, in press astro-ph/0412286
Ehle M, Dahlem M, Jiménez Bailón E, Santos-Lleó M, Read AM. 2004. IAU Symp #217, Recycling Intergalactic and Interstellar Medium, held in Sydney, Australia, Ed P-A Duc J Braine and E Brinks, 154. San Francisco: ASP
Ekers RD, Sancisi R. 1977:A&A 54:973
Ellis RS, Santos MR, Kneib J.-P, Kuijken K. 2001. ApJ 560:L119
Ellison SL, Mallén-Ornelas G, Sawicki M. 2003. ApJ 589:709
Ellison SL, Songaila A, Schaye J, Pettini M. 2000. AJ 120:1175
Elmouttie M, Haynes RF, Jones KL, Sadler EM, Ehle M. 1998. MNRAS 297:1202
Evrard A. E, Henry J. P 1991. ApJ 383:95
Fabian AC. 1999. MNRAS 308:L39
Fabian AC, Sanders JS, Allen SW, Crawford CS, Iwasawa K. 2003. MNRAS 344:L43
Fabian AC, Sanders JS, Ettori S, Taylor GB, Allen SW, et al. 2000. MNRAS 318:L65
Falcke H, Malkan MA, Biermann PL. 1995. A&A 298:375
Falcke H, Wilson AS, Simpson C. 1998. ApJ 502:199
Ferland GJ, Netzer H. 1983. ApJ 264:105
Fernández-Soto A, Lanzetta KM, Chen H.-W. 2003. MNRAS 342:1215
Ferrara A, Shchekinov Yu. 1993. ApJ 417:595
Ferrara A, Tolstoy E. 2000. MNRAS 313:291
Ferrarese L, Merritt D. 2000. ApJ 539:L9
Ferruit P, Binette L, Sutherland RS, Pécontal E. 1997. A&A 322:73
Ferruit P, Mundell CG, Nagar NM, Emsellem E, Pécontal E, Wilson AS, Schinnerer E. 2004. MNRAS 352:1180
Figer DF, Becklin EE, McLean IS, Gilbert AM, Graham JR, et al 2000. ApJ 533:L49
Filippenko AV, Sargent WLW. 1992. AJ 103:28
Finoguenov A, Matsushita K, Böhringer H, Ikebe Y, Arnaud M. 2002. A&A 381:21
Ford HC, Dahari O, Jacoby GH, Crane PC, Ciardullo R. 1986. ApJ 311:L7
Francis PJ, Williger GM, Collins NR, Palunas P, Malumuth EM, et al. 2001. ApJ 554:1001
Franx M, Illingworth GD, Kelson DD, van Dokkum PG, Tran K.-V. 1997. ApJ 486:L75
Frogel J. 1988. ARA&A 26:51
Frye B, Broadhurst T, Benitez N. 2002. ApJ 568:558
Fujita A, Mac Low MM, Ferrara A, Meiksin A. 2004. ApJ 613:159
Fukugita MHogan C. J, Peebles P. J. E 1998. ApJ 503:518
Gallimore JF, Baum SA, O'Dea CP. 1996b. ApJ 464:198
Gallimore JF, Baum SA, O'Dea CP. 1997. Nature 388:852
Gallimore JF, Baum SA, O'Dea CP, Pedlar A. 1996a. ApJ 458:136
Garcia-Burillo S, Martin-Pintado J, Fuente A, Neri R. 2000. A&A 355:499
Garcia-Burillo S, Martin-Pintado J, Fuente A, Neri R. 2001. ApJ 563:L27
Garcia-Lorenzo B, Arribas S, Mediavilla E. 2001. A&A 378:787
Garcia-Lorenzo B, Mediavilla E, Arribas S. 1999. ApJ 518:190
Garnett DR. 2002. ApJ 581:1019
Gebhardt K, Bender R, Bower G, Dressler A, Faber SM, et al. 2000. ApJ 539:L13
Gelderman R, Whittle M. 1994. ApJS 91:491
Gentile G, Salucci P, Klein U, Vergani D, Kalberla P. 2004. MNRAS 351:903
Genzel R, Hollenbach D, Townes CH. 1994. Rep Prog Phys 57:417
Genzel R, Thatte N, Krabbe A, Kroker H, Tacconi-Garman LE. 1996. ApJ 472:153
Ghez A, Klein BL, Morris M, Becklin EE. 1998. ApJ 509:678
Ghez AM, Salim S, Hornstein SD, Tanner A, Lu JR, et al. 2005. ApJ 620:744
Giallongo E, Christiani S, D'Odorico S, Fontana A. 2002. ApJ 568:L9
Giavalisco M, Livio M, Bohlin RC, Macchetto FD, Stecher TP. 1996. AJ 112:369
Gonzalez Delgado RM, Leitherer C, Heckman TM, Lowenthal JD, Ferguson HC, Robert C. 1998. ApJ 495:698
Gordon KD, Witt AN, Friedmann BC. 1998. ApJ 498:522
Greve A. 2004. A&A 416:67
Griffiths RE, Ptak A, Feigelson ED, Garmire G, Townsley L, et al. 2000. Science 290:1325
Grimes JP, Heckman TM, Strickland D,

Ptak A. 2005. ApJ in press astro-ph/0503685
Groves BA, Cecil G, Ferruit P, Dopita MA. 2004. ApJ 611:786
Haehnelt MG, Natarajan P, Rees MJ. 1998. MNRAS 300:817
Hartquist TW, Dyson JE, Williams RJR. 1997. ApJ 482:182
Heckman TM. 2004. ASP Conf. Astrophysics in the Far Ultraviolet, held at University of Victoria, British Columbia, Canada, Ed G Sonneborn, HW Moos, and B-G Andersson, Vol. #???, in press astro-ph/0410383. San Francisco: ASP
Heckman TM, Armus L, Miley GK. 1987. AJ 93:276
Heckman TM, Armus L, Miley GK. 1990. ApJS 74:833
Heckman TM, Lehnert MD, Strickland DK, Armus L. 2000. ApJS 129:493
Heckman TM, Leitherer C. 1997. AJ 114:69
Heckman TM, Robert C, Leitherer C, Garnett DR, van der Rydt F. 1998. ApJ 503:646
Heckman TM, Sembach KR, Meurer GR, Leitherer C, Calzetti D, Martin CL. 2001b. ApJ 558:56
Heckman TM, Sembach KR, Meurer GR, Strickland DK, Martin CL, Calzetti D, Leitherer C. 2001a. ApJ 554:1021
Heinz S, Choi Y.-Y, Reynolds CR, Begelman MC. 2002. ApJ 569:L79
Hellsten U, Davé R, Hernquist L, Weinberg DH, Katz N. 1997. ApJ 487:482
Helsdon SF, Ponman TJ. 2000. MNRAS 315:356
Hernàndez-Monteagudo C, Genova-Santos R, Atrio-Barandela F. 2004. ApJ 613:L89
Hjelm M Lindblad PO. 1996. A&A 305:727
Ho LC, Ulvestad JS. 2001. ApJS 133:77
Hoopes CG, Heckman TM, Strickland DK, Howk JC. 2003. ApJ 596:L175
Hoopes CG, Heckman TM, Strickland DK, Seibert M, Madore BF, et al. 2005. ApJ 619:L99
Horner DJ, Mushotzky RF, Scharf CA. 1999. ApJ 520:78
Hoyle F, Fowler W. 1963. MNRAS 125:169
Hughes DH, Gear WK, Robson EI. 1994. MNRAS 270:641
Hughes DH, Robson EI, Gear WK. 1990. MNRAS 244:759
Hummel E. 1991. A&A 251:442
Hummel E, Beck R, Dahlem M. 1991. A&AS 87:309
Hummel E, Dettmar R.-J. 1990. A&A 236:33
Hunter DA, Gallagher JS, III 1997. ApJ 475:65
Hunter DA, Hawley WN, Gallagher JS, III 1993. AJ 106:1797
Huo ZY, Xia XY, Xue SJ, Mao S, Deng ZG. 2004. ApJ , 611:208
Ichikawa T, van Driel W, Aoki T, Soyano T, Tarusawa K, Yoshida S. 1994. ApJ 433:645
Innes DE, Giddings JR, Falle SAEG. 1987a. MNRAS 226:67
Innes DE, Giddings JR, Falle SAEG. 1987b. MNRAS 227:1021
Inoue AK, Iwata I, Deharveng JM, Buat V, Burgarella D. 2005. A&A , in press astro-ph/0501382
Irwin JA, English J, Sorathia B. 1999. AJ 117:2102
Irwin JA, Saikia DJ. 2003. MNRAS 346:977
Irwin JA, Saikia DJ, English J. 2000. AJ 119:1592
Irwin JA Seaquist ER, Taylor AR, Duric N. 1987. ApJ 313:L91
Iwasawa K, Wilson AS, Fabian AC, Young AJ. 2003. MNRAS 345:369
Jablonka P, Martin P, Arimoto N. 1996. AJ 112:1415
Johnson HE, Axford WI. 1971. ApJ 165:381
Kaiser N 1991. ApJ 383:104
Kaiser ME, Bradley LD, II Hutchings JB, Crenshaw DM, Gull TR, et al. 2000. ApJ 528:260
Kauffmann G, Heckman TM, White SDM, Charlot S, Tremonti C, et al. 2003. MNRAS 341:54
Keel, WC. 2005. AJ 129:1863
Kennicutt RCJr. 1998. ARA&A 36:189
Kim D.-C, Veilleux S, Sanders DB. 1998. ApJ 508:627
Kim W.-T, Narayan R. 2003a. ApJ 596:L139
Kim W.-T, Narayan R. 2003b. ApJ 596:889
King A. 2003. ApJ 596:L27
Kinkhabwala A, Sako M, Behar E, Kahn SM, Paerels F. 2002. ApJ 575:732
Kinney AL, Schmitt HR, Clarke CJ, Pringle JE, Ulvestad JS, Antonucci RRJ. 2000. ApJ 537:152
Klein RI, McKee CF, Colella P. 1994. ApJ 420:213
Kobulnicky HA, Zaritsky D. 1999. ApJ

511:118
Kollmeier JA, Weinberg DH, Davé R, Katz N. 2003. ApJ 594:75
Königl A, Kartje JF. 1994. ApJ 434:446
Koo B.-C, McKee CF. 1992a. ApJ 388:93
Koo B.-C, McKee CF. 1992b. ApJ 388:103
Kormendy J. 1985. ApJ , 295:73
Kormendy J, Gebhardt K. 2001. Texas Symposium on relativistic astrophysics, 20th, held in Austin, Texas, Ed JC Wheeler and H Martel, 586:363. New York, American Institute of Physics
Kormendy J, Kennicutt RC Jr. 2004. ARA&A 42:603
Koyama K, Awaka H, Kunieda H, Takano S, Tawara Y. 1989. Nature 339:603
Koyama K, Maeda Y, Sonobe T, Takeshima T, Tanaka Y, Yamauchi S. 1996. PASJ 48:249
Krabbe A, Genzel R, Eckart A, Najarro F, Lutz D, et al 1995. ApJ 447:L95
Krolik JH. 1999. ApJ 515:L73
Krolik JH, McKee CF, Tarter CB. 1981. ApJ 249:422
Kunth D, Mas-Hesse JM, Terlevich E, Terlevich R, Lequeux J, Fall SM. 1998. A&A 334:11
Lanfranchini GA, Matteucci F. 2004. MNRAS 351:1338
Larson RB. 1974. MNRAS 169:229
Lehnert MD, Heckman TM. 1995. ApJS 97:89
Lehnert MD, Heckman TM. 1996. ApJ 462:651
Lehnert MD, Heckman TM, Weaver KA. 1999. ApJ 523:575
Leitherer C, Robert C, Drissen L. 1992. ApJ 401:596
Leitherer C, Schaerer D, Goldader JD, González Delgado RM, Robert C, et al. 1999. ApJS 123:3
Lequeux J, Kunth D, Mas-Hesse JM, Sargent WLW. 1995. A&A 301:18
Levenson NA, Weaver KA, Heckman TM. 2001a. ApJS 133:269
Levenson NA, Weaver KA, Heckman TM. 2001b. ApJ 550:230
Lloyd-Davies EJ, Ponman TJ, Cannon DB. 2000. MNRAS 315:689
Loeb A, Barkana R. 2001. ARA&A 39:19
Loewenstein M. 2001. ApJ 557:573
Lowenthal JD, Koo DC, Guzman R, Gallego J, Phillips AC, et al. 1997. ApJ 481:673
Lutz D. 1998. IAU Symp #184, The central regions of the Galaxy and galaxies, held in Kyoto, Japan, Ed Y Sofue, 91. Dordrecht: Kluwer Academic Publishers
Lynden-Bell D. 1969. Nature 223:690
Lynds CR, Sandage AR. 1963. ApJ 137:1005
MacLow M.-M, Ferrara A. 1999. ApJ 513:142
MacLow M.-M, McCray R. 1988. ApJ 324:776
MacLow M.-M, McCray R, Norman ML. 1989. ApJ 337:141
Malkan M, Webb W, Konopacky Q. 2003. ApJ 598:878
Maller AH, Dekel A. 2002. MNRAS 335:487
Malumuth EM, Heap SR. 1994. AJ 107:1054
Marcum PM, O'Connell RW, Fanelli MN, Cornett RH, Waller WH, et al. 2001. ApJS 132:129
Marlowe AT, Heckman TM, Wyse RFG, Schommer R. 1995. ApJ 438:563
Martin CL. 1998. ApJ 506:222
Martin CL. 1999. ApJ 513:156
Martin CL. 2005. ApJ 621:227
Martin CL, Kobulnicky HA, Heckman TM. 2002. ApJ 574:663
Mateo ML. 1998. ARA&A 36:435
Mathews WG, Baker JC. 1971. ApJ 170:241
Mathews WG, Brighenti F. 2003. ARA&A 41:191
Matsushita S, Kawabe R, Kohno K, Matsumoto H, Tsuru TG, Vila-Vilaro B. 2004. ApJ 617:20
McCarthy PJ, Baum SA, Spinrad H. 1996. ApJS 106:281
McDowell JC, Clements DL, Lamb SA, Shaked S, Hearn NC, et al. 2003. ApJ 591:154
McNamara B. R, Wise M, Nulsen PEJ, David LP, Sarazin CL, et al 2000. ApJ 534:L135
McNamara B. R, Wise MW, Nulsen PEJ, David LP, Carilli CL, et al 2001. ApJ 562:L149
Melioli C, de Gouveia Dal Pino EM. 2004. A&A 424:817
Meurer GR. 2004. IAU Symp #217, Recycling Intergalactic and Interstellar Medium, held in Sydney, Australia, Ed P-A Duc J Braine and E Brinks, 287. San Francisco: ASP

Meurer GR, Heckman TM, Leitherer C, Kinney A, Robert C, Garnett DR. 1995. AJ 110:2665
Middelberg E, Roy AL, Nagar NM, Krichbaum TP, Norris RP, Wilson AS, Falcke H, et al. 2004. A&A 417:925
Miller KA, Stone JM. 2000. ApJ 534:398
Miller ST, Veilleux S. 2003a. ApJS 148:383
Miller ST, Veilleux S. 2003b. ApJ 592:79
Moore DW, Spiegel EA. 1968. ApJ 154:863
Morganti R, Oosterloo TA, Emonts BHC, van der Hulst JM, Tadhunter CN. 2003. ApJ 593:L69
Morganti R, Tsvetanov ZI, Gallimore J, Allen MG. 1999. A&AS 137:457
Morris M, Serabyn E. 1996. ARA&A 34:645
Morris SL, van den Bergh S. 1994. ApJ 427:696
Mundell CG, Wrobel JM, Pedlar A, Gallimore JF. 2003. ApJ 583:192
Murray N, Quataert E, Thompson TA. 2005. ApJ 618:569
Mushotzky RF, Scharf CA. 1997. ApJ 482:L13
Mushotzky R, Loewenstein M, Arnaud KA, Tamura T, Fukazawa Y, et al. 1996. ApJ 466:686
Muxlow TWB, Pedlar A, Wilkinson PN, Axon DJ, Sanders EM, de Bruyn AG. 1994. MNRAS 266:455
Narayan R, Medvedev MV. 2001. ApJ 562:L129
Najarro F, Krabbe A, Genzel R, Lutz D, Kudritzki RP, Hillier DJ. 1997. A&A 325:700
Navarro JF, Eke VR, Frenk CS. 1996. MNRAS 283:L72
Nelson CH, Whittle M. 1996. ApJ 465:96
Norman CA, Ikeuchi S. 1989. ApJ , 345:372
Nulsen PEJ, Fabian AC. 1997. MNRAS 291:425
O'Connell RW, Gallagher JS, III Hunter DA, Colley WN. 1995. ApJ 446:L1
O'Dea CP, de Vries WH, Koekemoer AM, Baum SA, Morganti R, Fanti R, Capetti A, et al. 2002. AJ 123:2333
Oey MS. 1996. ApJ 467:666
Oey MS, Massey P. 1995. ApJ 452:2100
Oey MS, Matson AM, Kern K, Walth GL. 2005. AJ 129:393
Ohyama Y, Taniguchi Y, Iye M, Yoshida M, Sekiguchi K, et al. 2002. PASJ 54:891
Ohyama Y, Taniguchi Y, Shioya Y. 2004. AJ 128:2704
Ohyama Y, Yoshida M, Takata T. 2003. AJ 126:2291
Oort JH. 1977:ARA&A 15:295
Oosterloo TA, Morganti R. 2005. A&A 429:469
Osterbrock DE. 1960. ApJ 132:325
Osterbrock DE. 1989. Astrophysics of Gaseous Nebulae and Active Galactic Nuclei (Mill Valley1: UnivSci.)
Ostriker JE, McKee CF. 1988. RevModPhys 60:1
Ott J, Walter F, Brinks E. 2005. MNRAS 358:1453
Otte B, Murphy EM, Howk JC, Wang QD, Oegerle WR, Sembach KR. 2003. ApJ 591:821
Pedlar A, Dyson JE, Unger SW. 1985. MNRAS 214:463
Perrin J.-M, Darbon S, Sivan J.-P. 1995. A&A 304:L21
Persic M, Salucci P, Stel F. 1996. MNRAS 281:27
Pettini M, Kellogg M, Steidel CC, Dickinson M, Adelberger KL, Giavalisco M. 1998, ApJ 508:539
Pettini M, Madau P, Bolte M, Prochaska JX, Ellison SL, Fan X. 2003. ApJ 594:695
Pettini M, Rix S, A, Steidel CC, Adelberger KL, Hunt MP, Shapley AE. 2002. ApJ 569:742
Pettini M, Shapley AE, Steidel CC, Cuby J.-G, Dickinson M, et al. 2001. ApJ 554:981
Pettini M, Steidel CC, Adelberger KL, Dickinson M, Giavalisco M. 2000. ApJ 528:96
Phillips AC. 1993. AJ 105:486
Pier EA, Krolik JH. 1992. ApJ 401:99
Pietsch W, Vogler A, Klein U, Zinnecker H. 2000. A&A 360:24
Pildis RA, Bregman JN, Schombert JM. 1994. ApJ 427:160
Pogge RW. 1988. ApJ 328:519
Poludnenko AY, Frank A, Blackman EG. 2002. ApJ 576:832
Popescu CC, Tuffs RJ, Fischera J, Völk H. 2000. A&A 354:480
Puche D, Westpfahl D, Brinks E, Roy JR. 1992. AJ 103:1841
Qian YZ, Wasserburg GJ. 2005. ApJ 623:17
Radovich M, Kahanpää J, Lemke D. 2001. A&A 377:73
Rand RJ. 1996. ApJ 462:712
Rand RJ, Kulkarni SR, Hester JJ. 1992.

ApJ 396:97
Rauch M. 1998. ARA&A 36:267
Rauch M, Haehnelt MG, Steinmetz M. 1997. ApJ 481:601
Rauch M, Sargent WLW, Barlow TA, Simcoe RA. 2002. ApJ 576:45
Read JI, Gilmore G. 2005. MNRAS 356:107
Read AM, Ponman TJ, Strickland DK. 1997. MNRAS 286:626
Redman MP, Al-Mostafa ZA, Meaburn J, Bryce M. 2003. MNRAS 344:741
Reid MJ. 1993. ARA&A 31:345
Renzini A. 2004. Clusters of Galaxies: Probes of Cosmological Structure and Galaxy Evolution, held at the Carnegie Observatories, Pasadena, California, Eds JS Muchaey, A Dressler and A Oemler, p. 261. Cambridge: Cambridge University Press
Reynolds CS, McKernan B, Fabian AC, Stone JM, Vernaleo JC. 2005. MNRAS 357:242
Ricotti M, Wilkinson MI. 2004. MNRAS 353:867
Rieke GH, Lebofsky MJ, Thompson RI, Low FJ, Tokunaga AT. 1980. ApJ 238:24
Rossa J, Dettmar R.-J. 2000. A&A 359:433
Rossa J, Dettmar R.-J. 2003a. A&A 406:493
Rossa J, Dettmar R.-J. 2003b. A&A 406:505
Rossa J, Dettmar R.-J, Walterbos RAM, Norman CA. 2004. AJ 128:674
Ruiz JR, Crenshaw DM, Kraemer SB, Bower GA, Gull TR, et al. 2001. AJ 122:2961
Ruiz JR, Crensahw DM, Kraemer SB, Bower GA, Gull TR, et al. 2005. AJ 129:73
Rupke DS Veilleux S, Sanders DB. 2002. ApJ 570:588
Rupke DS Veilleux S, Sanders DB. 2005a. ApJ in press
Rupke DS Veilleux S, Sanders DB. 2005b. ApJ in press
Rupke DS Veilleux S, Sanders DB. 2005c. ApJ submitted
Ruszkowski M, Begelman MC. 2002. ApJ 581:223
Ruszkowski M, Brüggen M, Begelman MC. 2004a. ApJ 611:158
Ruszkowski M, Brüggen M, Begelman MC. 2004b. ApJ 615:675
Sahu MS, Blades JC. 1997. ApJ 484:L125
Saito M. 1990. PASJ 42:19
Sakamoto K, Scoville NZ, Yun MS, Crosas M, Genzel R, Tacconi LJ. 1999. ApJ 514:68
Salzer JJ, Lee JC, Melbourne J, Hinz JL, Alonso-Herrero A, Jangren A. 2005. AJ in press astro-ph/0502202
Sanders DB, Phinney ES, Neugebauer G, Soifer BT, Matthews K. 1989. ApJ 347:29
Sanders RH. 1989. IAU Symp. #136, The Center of the Galaxy, held in Los Angeles, California, ed M Morris, p. 77. Dordrecht: Kluwer Academic Publishers
Sanders RH, Prenderghast KH. 1974. ApJ 188:489
Scannapieco E, Broadhurst T. 2001. ApJ 549:28
Scannapieco E, Thacker RJ, Davis M. 2001. ApJ 557:605
Scarrott SM, Eaton N, Axon DJ. 1991. MNRAS 252:12P
Scarrott SM, Draper PW, Stockdale DP, Wolstencroft RD. 1993. MNRAS 264:L7
Scheuer PAG. 1974. MNRAS 166:513
Schiano AVR. 1985. ApJ 299:24
Schiano AVR, Christiansen WA, Knerr JM. 1995. ApJ 439:237
Schmidt GD, Angel JRP, Cromwell RH. 1976. ApJ 206:888
Schmitt HR, Donley JL, Antonucci RRJ, Hutchings JB, Kinney AL. 2003a. ApJS 148:327
Schmitt HR, Donley JL, Antonucci RRJ, Hutchings JB, Kinney AL, Pringle JE. 2003b. ApJ 597:768
Schödel R, Ott T, Genzel R, Eckart, A, Mouawad N, Alexander T. 2003. ApJ 596:1015
Schwartz CM, Martin CL. 2004. ApJ 610:201
Seaquist ER, Clark J. 2001. ApJ 552:133
Seaquist ER, Odegard N. 1991. ApJ 369:320
Sedov L. 1959. Similarity and Dimensional Methods in Mechanics, New York: Academic Press.
Shapley AE, Steidel CC, Pettini M, Adelberger KL. 2003. ApJ 588:65
Shen J, Lo KY. 1995. ApJ 445:L99
Shopbell PL, Bland-Hawthorn J. 1998. ApJ 493:129
Shull JM, Saken JM. 1995. ApJ 444:663
Silich SA, Franco J, Palous J, Tenorio-

Tagle G. 1996. ApJ 468:722
Silich SA, Tenorio-Tagle G. 2001. ApJ 552:91
Silich STenorio-Tagle G, Muñoz-Tuñón C. 2003. ApJ 590:791
Silk J. 2003. MNRAS 343:249
Silk J, Rees MJ. 1998. A&A 331:L1
Simpson JP, Witteborn FC, Cohen M, Price SD. 1999. ASP Conf. The Central Parsecs of the Galaxy, held in Tucson, Arizona, Vol. #186, Eds H Falcke et al, p. 527. San Francisco: ASP
Sjouwerman LO, Habing HJ, van Langevelde HJ, Lindqvist M, Winnberg A. 1998. IAU Symp. #184, The Central Regions of the Galaxy and Galaxies, held in Kyoto, Japan, ed Y Sofue, IAU Symp 184, p. 129. Dordrecht: Kluwer Academic Publishers
Smail I, Chapman SC, Ivison RJ, Blain AW, Takata T, et al. 2003. MNRAS 342:1185
Smith DA, Wilson AS. 2001. ApJ 557:180
Smith MD, Smarr L, Norman ML, Wilson JR. 1983. ApJ 264:432
Sofue Y, Handa T. 1984. Nature 310:568
Sofue Y, Wakamatsu K.-I, Malin DF. 1994. AJ 108:2102
Solórzano-Iñarrea C, Tadhunter CN, Axon DJ. 2001. MNRAS 323:965
Somerville RS, Primack JR. 1999. MNRAS 310:1087
Sommer-Larsen J, Götz M, Portinari L. 2003. ApJ 596:47
Songaila A. 1997. ApJ 490:L1
Songaila A. 2001. ApJ 561:L153
Spitzer LJr. 1956:ApJ 124:20
Spitzer LJr. 1990. ARA&A 28:71
Springel V, Hernquist L. 2003. MNRAS 339:289
Stark AA, Carlson ER. 1984. ApJ 279:122
Steffen W, Gomez JL, Williams RJR, Raga AC, Pedlar A. 1997a. MNRAS 286:1032
Steffen W, Gomez Raga AC, JL, Williams RJR. 1997b. ApJ 491:L73
Steidel CC, Hunt MP, Shapley AE, Adelberger KL, Pettini M, Dickinson M, Giavalisco M. 2002. ApJ 576:653
Steidel CC, Pettini M, Adelberger KL. 2001. ApJ 546:665
Steigman G, Strittmatter PA, Williams RE. 1975. ApJ 198:575
Steinmetz M, Navarro JF. 1999. ApJ 513:555
Stevens IR, Hartwell JM. 2003. MNRAS 339:280
Stevens IR, Read AM, Bravo-Guerrero J. 2003. MNRAS 343:L47
Stewart S G, Fanelli M N, Byrd G G, Hill J K, Westpfahl D J, et al. 2000. ApJ , 529:201
Stickel M, Klaas U, Lemke D, Mattila K. 2002. A&A 383:367
Stickel M, Lemke D, Mattila K, Haikala LK, Haas M. 1998. A&A 329:55
Strickland DK, Heckman TM, Weaver KA, Dahlem M. 2000. AJ 120:2965
Strickland DK, Heckman TM, Weaver KA, Hoopes CG, Dahlem M. 2002. ApJ 568:689
Strickland DK, Heckman TM, Colbert EJM, Hoopes CG, Weaver KA. 2004a. ApJS 151:193
Strickland DK, Heckman TM, Colbert EJM, Hoopes CG, Weaver KA. 2004b. ApJ 606:829
Strickland DK, Stevens IR. 2000. MNRAS 314:511
Suchkov A, Balsara DS, Heckman TM, Leitherer C. 1994. ApJ 430:511
Suchkov A, Berman VG, Heckman TM, Balsara DS. 1996. ApJ 463:528
Sugai H, Davies RI, Ward MJ. 2003. ApJ : 584:L9
Summers LK, Stevens IR, Strickland DK, Heckman TM. 2003. MNRAS 342:690
Sutherland RS, Bicknell GV, Dopita MA. 2003a. ApJ 591:238
Sutherland RS, Bisset DK, Bicknell GV. 2003b. ApJS 147:187
Swinbank, M, Smail I, Bower R, Borys C, Chapman S, et al. 2005. MNRAS 359:401
Tadhunter CN. 2002. RMxAC 13:213
Tamblyn P, Rieke GH. 1993. ApJ 414:573
Tamura T, Kaastra JS, den Herder JWA, Bleeker JAM, Peterson JR. 2004. A&A 420:135
Taylor CL Walter F, Yun MS. 2001. ApJ 562:L43
Taylor D, Dyson JE, Axon DJ. 1992. MNRAS 255:351
Taylor G. 1950. ProcRoySocLondon A 201:159
Tenorio-Tagle G, Bodenheimer P. 1988. ARA&A 26:145
Tenorio-Tagle G, Muñoz-Tuñón C. 1997. ApJ 478:134
Tenorio-Tagle G, Muñoz-Tuñón C. 1998.

MNRAS 293:299
Tenorio-Tagle G, Silich SA, Kunth D, Terlevich E, Terlevich R. 1999. MNRAS 309:332
Theuns T, Viel M, Kay S, Schaye J, Carswell RF, Tzanavaris P. 2002. ApJ 578:L5
Thornton K, Gaudlitz M, Janka H.-Th, Steinmetz M. 1998. ApJ 500:95
Tomisaka K, Bregman JN. 1993. PASJ 45:513
Tomisaka K, Ikeuchi S. 1988. ApJ 330:695
Trager SC, Worthey G, Faber SM, Burstein D, Gonzalez JJ. 1998. ApJS 116:1
Tremaine S, Gebhardt K, Bender R, Bower G, Dressler A, Faber SM, et al. 2002. ApJ 574:740
Tremonti CA, Heckman TM, Kauffmann G, Brinchmann J, Charlot S, et al. 2004. ApJ 613:898
Ulvestad JS, Ho LC. 2001. ApJ 558:561
Ulvestad JS, Wilson AS. 1984. ApJ 285:439
Ulvestad JS, Wilson AS. 1989. ApJ 343:659
Vader JP. 1986. ApJ 305:669
van Breugel W, Filippenko AV, Heckman T, Miley G. 1985. ApJ 293:83
van Breugel WJ, Fragile C, Anninos P, Murray S. 2004. IAU Symp #217, Recycling Intergalactic and Interstellar Medium, held in Sydney, Australia, Ed P-A Duc J Braine and E Brinks, 472. San Francisco: ASP
van den Bosch FC. 2001. MNRAS 327:1334
van den Bosch FC, Swaters RA. 2001. MNRAS 325:1017
van der Kruit PC. 1971. A&A 13:405
van Woerden H, Rougoor GW, Oort JH. 1957. Comptes Rendus 244:1691
Veilleux S. 1991. ApJ 369:331
Veilleux S. 2001. Starburst Galaxies: Near and Far, Eds L Tacconi and D Lutz, Springer-Verlag, 88
Veilleux S, Bland-Hawthorn J. 1997. ApJ 479:L105
Veilleux S, Bland-Hawthorn J, Cecil G, Tully RB, Miller ST. 1999. ApJ 520:111
Veilleux S, Cecil G, Bland-Hawthorn J, Shopbell PL. 2002a. RMxAC 13:222
Veilleux S, Cecil G, Bland-Hawthorn J, Tully RB, Filippenko AV, Sargent WLW. 1994. ApJ 433:48
Veilleux S, Kim D.-C, Sanders DB. 2002b. ApJS 143:315
Veilleux S, Kim D.-C, Sanders DB, Mazzarella JM, Soifer BT. 1995. ApJS 98:171
Veilleux S, Osterbrock DE. 1987. ApJS 63:295
Veilleux S, Rupke DS. 2002. ApJ 565:L63
Veilleux S, Shopbell PL, Miller ST. 2001. AJ 121:198
Veilleux S, Shopbell PL, Rupke DS, Bland-Hawthorn J, Cecil G. 2003. AJ 126:2185
Vietri M, Ferrara A, Miniati F. 1997. ApJ 483:262
Voit GM. 1994. ApJ 432:L19
Wada K, Norman CA. 2001. ApJ 547:172
Walter F, Weiss A, Scoville N. 2002. ApJ 580:L21
Wang QD, Gotthelf EV, Lang CC. 2002. Nature 415:148
Weaver R, McCray R, Castor J, Shapiro P, Moore R. 1977:ApJ 218:377
Wehrle AE, Morris M. 1988. AJ 95:1689
Whittle M. 1985. MNRAS 213:1
Whittle M. 1992a. ApJ 387:109
Whittle M. 1992b. ApJ 387:121
Whittle M, Wilson AS. 2004. AJ 127:606
Williams RJR, Dyson JE. 2002. MNRAS 333:1
Willott CJ, Rawlings S, Blundell KM, Lacy M. 1999. MNRAS 309:1017
Wills KA, Redman MP, Muxlow TWB, Pedlar A. 1999. MNRAS 309:395
Wilson AS. 1981. ESO/ESA Workshop #2, Optical Jets in Galaxies, held in Garching, Germany, ESA SP-162, Ed B. Battick and J Mort, p. 125. Paris: ESA
Wilson AS, Baldwin JA, Ulvestad JS. 1985. ApJ 291:627
Wilson AS, Heckman TM. 1985. in Astrophysics of Active Galaxies and Quasi-Stellar Objects (Mill Valley1: UnivSci.) 39
Wilson AS, Tsvetanov ZI. 1994. AJ 107:1227
Wilson AS, Ward MJ, Haniff CA. 1988. ApJ 334:121
Wilson AS, Willis AG. 1980. ApJ 240:429
Wilson AS, Yang Y, Cecil G. 2001. ApJ 560:689
Woosley SE, Weaver TA. 1995. ApJS 101:181
Worrall DM, Birkinshaw M. 2004. Physics of Active Galactic Nuclei at all Scales, Eds D Alloin, R Johnson, and P Lira (Springer Verlag) astro-ph/0410297
Wyse RFG, Silk J. 1985. ApJ 296:L1
Yamauchi S, Kawada M, Koyama K, Ku-

nieda H, Tawara Y. 1990. ApJ 365:532
Yang Y, Wilson AS, Ferruit P. 2001. ApJ 563:124
Young AJ, Wilson AS, Shopbell PL. 2001. ApJ 556:6
Yusef-Zadeh F, Cotton W, Hewitt J, Law C, Maddalena R, Roberts DA. 2005. in press. astro-ph/0501316
Yusef-Zadeh F, Melia F, Wardle M. 2000. Science 287:85
Zaritsky D, Gonzalez AH, Zabludoff AI. 2004. ApJ 613:L93
Zaritsky D, Kennicutt RC Jr, Huchra JP. 1994. ApJ 420:87
Zensus JA. 1997. ARA&A 35:607
Zonak SG, Charlton JC, Ding J, Churchill CW. 2004. ApJ 606:196